Check for updates

JGR Solid Earth

RESEARCH ARTICLE
10.1029/2021JB022211

Geodetic Datum Realization Using SLR-GNSS Co-Location Onboard Galileo and GLONASS

G. Bury[1], K. Sośnica[1], R. Zajdel[1], D. Strugarek[1], and U. Hugentobler[2]

[1]Institute of Geodesy and Geoinformatics, Wrocław University of Environmental and Life Sciences, Wroclaw 50-357, Poland, [2]Institute for Astronomical and Physical Geodesy, Technical University of Munich, Munich, Germany

Key Points:

- Co-location of Satellite Laser Ranging (SLR) and Global Navigation Satellite Systems (GNSS) space techniques onboard navigation satellites enables the realization of a terrestrial reference frame in space
- Space ties computed using GNSS and SLR observations indicate a 1-mm consistency with local ties for co-located SLR and GNSS stations
- Different methods of the handling of SLR range biases lead to different realizations of the terrestrial reference frame origin and scale

Supporting Information:

Supporting Information may be found in the online version of this article.

Correspondence to:

G. Bury,
grzegorz.bury@upwr.edu.pl

Citation:

Bury, G., Sośnica, K., Zajdel, R., Strugarek, D., & Hugentobler, U. (2021). Geodetic datum realization using SLR-GNSS co-location onboard Galileo and GLONASS. *Journal of Geophysical Research: Solid Earth*, *126*, e2021JB022211. https://doi.org/10.1029/2021JB022211

Received 9 APR 2021
Accepted 29 SEP 2021

Author Contributions:

Conceptualization: G. Bury, K. Sośnica, U. Hugentobler
Data curation: G. Bury
Formal analysis: G. Bury
Funding acquisition: K. Sośnica
Investigation: U. Hugentobler
Methodology: G. Bury
Software: G. Bury, R. Zajdel
Supervision: K. Sośnica, U. Hugentobler

© 2021. The Authors.
This is an open access article under the terms of the Creative Commons Attribution-NonCommercial-NoDerivs License, which permits use and distribution in any medium, provided the original work is properly cited, the use is non-commercial and no modifications or adaptations are made.

Abstract Modern satellites of Global Navigation Satellite Systems (GNSS) are equipped with laser retroreflector arrays for Satellite Laser Ranging (SLR). Laser range observations to GNSS satellites allow for the co-location of two space geodetic techniques onboard navigation satellites. We search for the best network constraining strategy for the SLR and GNSS stations to realize the geodetic datum using combined microwave-GNSS and SLR-to-GNSS measurements. We find that consistent imposing of no-net-translation and no-net-rotation for the unified GNSS and SLR network provides the best quality of station coordinates and the best common realization of the terrestrial reference frame (TRF). We employ the space ties using solely space geodetic techniques for the SLR and GNSS station coordinates and confront them with the ground-based measurements, that is, local ties, conducted at the SLR-GNSS co-located sites. The common processing of the GNSS and SLR observations allows for the realization of the TRF using space ties that are independent of the a priori coordinates and independent of the errors in local tie measurements. The agreement of space ties with ground measurements is at the level of 1 mm in terms of long-term mean values for the co-located station in Zimmerwald, Switzerland. We also revise the approach for handling the SLR range biases which now considers the impact of the SLR observations to GNSS and LAGEOS satellites. The updated SLR range biases improve the agreement between space ties and local ties from 4.4 to 2.4 mm for the co-located station in Wettzell, Germany.

Plain Language Summary Every natural phenomenon observed in the Earth system demands a stable and accurate terrestrial reference frame (TRF). Currently, TRF is resolved by a combination of observations provided solely by space techniques, that is, Global Navigation Satellite Systems (GNSS), Satellite Laser Ranging (SLR), Very Long Baseline Interferometry (VLBI), and Doppler Orbitography and Radiopositioning Integrated by Satellite (DORIS). All the techniques are treated separately in the current realization of the International Terrestrial Reference Frame (ITRF2014), and a linkage between the observing stations of each technique is resolved by ground measurements as the so-called "local ties" which cannot be obtained operationally. However, newly developed satellites of GNSS systems are equipped with laser retroreflectors for the SLR technique. As a result, the GNSS satellites comprise a platform for the integration of two techniques onboard navigation spacecraft in space. This study provides the first-ever results of co-location onboard navigation satellites of the Galileo and GLONASS systems. The new linkage between the GNSS and SLR techniques called "space tie" is consistent with local ties at the level of 1 mm and can be provided whenever GNSS and SLR data are available enabling, therefore, the realization of TRF in space on the operational basis.

1. Introduction

Satellites of the modernized and new emerging Global Navigation Satellite Systems (GNSS) are equipped with laser retroreflector arrays (LRA) for Satellite Laser Ranging (SLR). Alongside the Very Long Baseline Interferometry (VLBI) and Doppler Orbitography and Radiopositioning Integrated by Satellite (DORIS), GNSS and SLR contribute to the realization of the International Terrestrial Reference Frame (ITRF, Altamimi et al., 2016). Currently, the integration of all geodetic techniques is realized using local ties which are derived based on *in situ* measurements between reference points of SLR telescopes, GNSS, DORIS, and VLBI antennae using geodetic instruments, such as tachymetry and precise leveling corrected by local plumb line deflections (Glaser et al., 2015; Sarti et al., 2013). Even three space geodetic techniques (DORIS, GNSS, SLR) are already co-located onboard altimeter satellites (since 2001 with Jason-1) and their contribution is also neglected in ITRF realizations. Moreover, laser ranging to GNSS is currently neglected in ITRF.

Validation: G. Bury, R. Zajdel, D. Strugarek, U. Hugentobler
Visualization: G. Bury
Writing – original draft: G. Bury

SLR observations to GNSS are mainly used to validate the microwave-based orbit products (Sośnica et al., 2020; Zajdel et al., 2017). However, laser ranging to GNSS satellites allows for independent precise GNSS orbit determination using solely SLR data (Bury et al., 2019) or determination of global geodetic parameters such as station coordinates, Earth rotation parameters (ERPs), global scale, and geocenter coordinates (GCC; Sośnica et al., 2018). SLR observations to GNSS satellites are especially beneficial for the determination of SLR station coordinates for those stations that are focused on tracking GNSS satellites, because the determination efficiency of the coordinates of such stations increases by over 40% (Sośnica et al., 2019).

Finally, when using combined GNSS and SLR observations to the navigation satellites one can provide the co-location of the two techniques onboard the satellites to realize the geodetic reference frame with the determination of the global geodetic parameters (Glaser et al., 2020). The impact of the combined GNSS and SLR-to-GNSS observations on the precise Galileo orbit determination was evaluated by Bury et al. (2021). The combination of the SLR observations with the microwave GNSS data improved the quality of the Galileo orbits especially, for the period when the elevation of the Sun above the orbital plane is higher than 60°. In such cases of the Sun-Earth-satellite geometry, the stability of the orbit solution is constrained by the laser range measurements which contribute mainly to the improvement of the orbit radial direction.

The co-location onboard GNSS satellites allows for the realization of the terrestrial reference frame (TRF) using the so-called space ties. The space tie is possible when two instruments for independent techniques are co-located on the same spacecraft (see Figure 1). The space tie vector can be defined between the phase center of the GNSS antenna transmitter and the centroid of the SLR LRA onboard the satellite. Space ties are not directly measured, yet they implicitly provide the linkage between SLR and GNSS observations and therefore comprise an independent connection from the ground measurements (Figure 1). Moreover, local ties can link only the co-located SLR and GNSS stations (Kodet et al., 2018; Pinzón & Rothacher,, 2020). The space ties, however, might be considered also for not co-located GNSS and SLR stations placed in different locations. The only condition that has to be fulfilled is the availability of the GNSS and SLR observations referred to the same GNSS satellite.

Many studies raise the subject of possible co-location in space for different space techniques. However, most of them are based on simulated data, yet they indicate the advantage of the space ties over the inter-technique linkage on the ground (Anderson et al., 2018; Glaser et al., 2019; Klopotek et al., 2020).

Thaller et al. (2011) conducted the co-location onboard navigation satellites using SLR observations to GLONASS and the only pair of GPS satellites equipped with LRAs. When imposing the minimum constraints on the translation (no-net-translation, NNT) and rotation (no-net-rotation, NNR) on a sub-set of stable GNSS stations, Thaller et al. (2011) determined the SLR station coordinates as free parameters with an accuracy at the level of 1–2 cm. Further studies by Thaller et al. (2014, 2015) incorporated additionally the SLR observations to the dedicated geodetic satellites, that is, LAGEOS and Etalon. Bruni et al. (2018) computed the space ties using combined microwave GPS and GLONASS, SLR-to-GNSS, and SLR-to-LAGEOS observations. However, they failed to transfer either the TRF scale or origin information using a combination of these data. The major limiting factors of space ties onboard GLONASS and GPS include modeling issues of precise orbits and the lack of microwave antenna calibrations onboard satellites.

For the past two decades, when the only GNSS equipped with LRAs were the GLONASS constellation and the single pair of GPS satellites, the co-location might not have given satisfying results. Nowadays, the Galileo system with 24 satellites equipped with LRAs, introduces a new opportunity for the realization of the TRF using combined GNSS and SLR-to-GNSS observations. Moreover, the methodology of the space ties computation should be revised as the results obtained by Bruni et al. (2018) might not be satisfying due to the fact of pre-elimination of the orbit parameters, employing an obsolete GNSS orbit model, estimating antenna offsets as additional parameters, or suboptimal handling of the SLR range biases (RB). In the current realization of the ITRF2014, the SLR technique is used for the realization of the origin and the scale (the latter together with VLBI), which are then transferred to other techniques using station local ties (Altamimi et al., 2016). GNSS satellites have the full potential to sense the origin of the reference frame, because the GNSS satellites orbit around the instantaneous position of the Earth center-of-mass, and the scale of the reference frame, provided that the GNSS antennae are properly calibrated. Thus, the space ties should provide the same TRF connection opportunities as local ties in terms of the transfer of the scale, origin, and

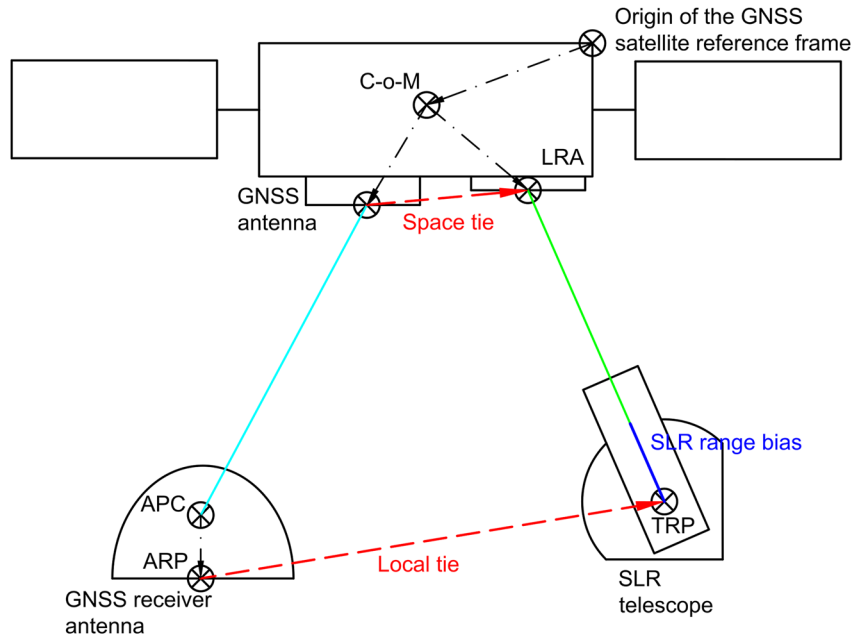

Figure 1. Co-location onboard GNSS satellite scheme. Cyan, green, and blue lines denote microwave, laser ranging observation, and SLR range bias, respectively. APC denote GNSS antenna phase center, APR–GNSS antenna reference point, TRP–SLR telescope reference point, LRA–laser retroreflector array, C-o-M–GNSS satellite center-of-mass.

orientation of the reference frames and even in terms of providing a common realization of the TRF origin, orientation, and scale through the connections onboard satellites (Figure 1).

1.1. Goal of This Study

The goal of this study is to derive the best TRF realization strategy using co-location onboard Galileo and GLONASS satellites. We test different approaches for the GNSS and SLR network constraints and evaluate the possibility of space tie realization by incorporating observations solely to the GNSS satellites, that is, microwave–broadcasted by the satellites, and optical–conducted by the SLR ground stations. Moreover, we assess the strength and robustness of the determined space ties. We compute a series of combined GNSS and SLR strategies estimating global geodetic parameters, that is, station coordinates, GNSS orbit parameters, ERPs, and GCC. Finally, we check whether it is possible to determine reliable GCC and ERPs using GNSS observations combined with SLR observations to the navigation satellites. Therefore, apart from employing the space ties, we also employ the global ties, that is, the GNSS-SLR connection, by estimating common global geodetic parameters: ERPs and the geocenter motion in different configurations of 1-day solutions.

2. Methodology

The realization of the geodetic datum using co-location onboard navigation satellites requires a uniform network of sites representing GNSS and SLR techniques. Before the combination of the two techniques, the technique-specific normal equation systems (NEQ) are prepared. All solutions are computed in a modified version of the Bernese GNSS Software v.5.2 (Dach et al., 2015), which is prepared for the handling of network constraining separately for each space geodetic technique. For both techniques, we determine 1-day NEQs for each day for the period between 2017.0 and 2019.0.

2.1. GNSS Solution

Processing of the microwave-GNSS data is based on the ionospheric-free linear combination of the double-difference GPS + GLONASS + Galileo observations collected by the global GNSS network following the strategy elaborated by Zajdel, Sośnica, Dach, et al. (2019). The GNSS observations are collected by

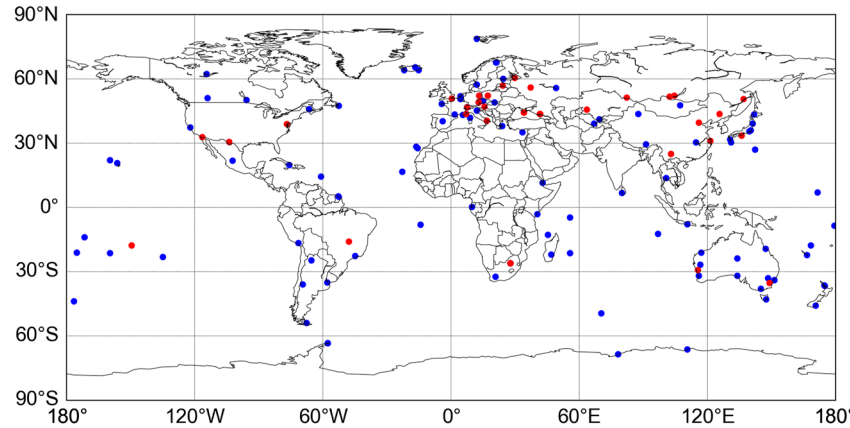

Figure 2. Distribution of GNSS (blue) and SLR (red) stations considered in the processing.

approximately 100 globally distributed sites (see Figure 2) referred to the IGS14, which is the International GNSS Service's (IGS, Johnston et al., 2017) realization of the ITRF2014 with the same origin, orientation, and scale (Rebischung et al., 2016). The solution based solely on the microwave GNSS data is called *M*1 (see Table 3) and comprises the reference for the GNSS network in terms of the TRF realization. The solution *M*1 is computed by imposing NNT and NNR constraints, with the estimation of the GCC. The minimum constraints are applied to the set of stable stations which are checked using Helmert transformation in the pre-processing stage for each 1-day solution (Zajdel, Sośnica, Dach, et al., 2019).

2.2. SLR-To-GNSS Solution

Concerning the SLR observations to GNSS, we apply the methodology developed by Bury et al. (2019). The SLR-based NEQs, are calculated using direct range measurements based on the fixed microwave-based GNSS orbits. In contrast to the GNSS solution, we do not derive an SLR-only solution as the number of SLR observations to GNSS is insufficient within a 1-day interval; the SLR-based NEQs cannot be inverted and are only saved for the combination with the GNSS-based NEQs. The a priori SLR station coordinates are referred to the SLRF2014 (Luceri et al., 2019), which is the International Laser Ranging Service's (ILRS, Pearlman et al., 2019) realization of the ITRF2014 with the same origin, orientation, and scale. SLR processing demands coping with SLR RBs. In this study, as the main approach, we use an analogous one as proposed by Appleby et al. (2016), estimating annual mean RBs for each satellite-station pair, and then resubstituting them as a priori values for the final processing. The main approach for the RBs computation considers only SLR observations to GNSS satellites with fixed orbits and station coordinates. The estimated RBs should absorb any uncertainties resulting from the LRA offsets and instrument-related biases; hence in the processing, we do not estimate LRA offsets. Additionally, we compute two experimental RB solutions in which not only the impact of SLR-to-GNSS observations but also SLR observations to LAGEOS satellites and the microwave-GNSS data are considered. Further details are described in Section 3.4.

2.3. Combined GNSS and SLR Solution

The combined solution is obtained based on the combination of GNSS and SLR NEQs, which are referred to different datums. The differences between IGS14 and SLRF2014 are proved to be negligible based on the combination of SLR and GNSS data onboard Sentinel-3A/B satellites (Strugarek et al., 2019). Henceforth, all the GNSS and SLR sites are considered as a common and consistent network with the possibility of imposing different constraints on each set of sites. In this study, we test a number of strategies in which we impose a different set of minimum constraints for each GNSS and SLR network (see Table 3). The combined solution is conducted epoch-wise independently for each one day of the period 2017.0–2019.0 like in the case of epoch-wise filtered TRF realization proposed by Abbondanza et al. (2017). In such a manner, it is possible to determine the epoch-specific global geodetic parameters as well as the GNSS satellite orbits (Prange et al., 2020). Concerning the GNSS, the set of stations is consistent with the solution *M*1, whereas,

Table 1
List of Models for GNSS and SLR Data Processing

Component	GNSS	SLR
Troposphere	Dry part: Vienna Mapping Function (Böehm et al., 2006), wet part: estimated (see Table 2)	Dry and wet based on meteorological data (Mendes & Pavlis, 2004)
Ionosphere	Ionospheric-free linear combination and modeling of higher-order terms and bending effect (Hadas et al., 2017)	-
Reference frame	IGS14 (Rebischung et al., 2016)	SLRF2014 (Luceri et al., 2019)
Sat. antenna model	Phase center offsets (PCO) and phase center variations (PCV) for GPS and GLONASS	-
	PCO for Galileo; based on CODE MGEX ANTEX (http://ftp.aiub.unibe.ch/CODE_MGEX/CODE/M14.ATX)	
Rec. antenna model	GPS, GLONASS: IGS14 Galileo: Adopted from GPS L1 and L2	-
Observation sampling	180 s	Normal points formulated out of 300 s raw SLR data
LRA offsets	-	Galileo metadata
Earth Gravity Model	EGM2008 (Pavlis et al., 2012)	
Earth Orientation	A priori ERP: IERS-C04-14 (Bizouard et al., 2019)	
Solid Earth tides	IERS2010 (Petit & Luzum, 2010)	
Ocean Tides	FES2004 (Lyard et al., 2006)	
Ocean tidal loading and geocenter corrections	FES2004, provided by Scherneck (1991)	
Solid Earth pole tides	IERS2010 based on Desai (2002)	
Mean Pole definition	IERS2010 Petit and Luzum (2010)	
Solar radiation pressure	A priori box-wing model based on the Galileo metadata (Bury et al., 2020)	
Albedo + infrared radiation	CERES monthly maps (Wielicki et al., 1996)	
Antenna thrust	IOV: 155 W, FOC: 200 W (Steigenberger et al., 2018)	

for the SLR, we impose the constraints for the reduced core station list consistently with Zajdel, Sośnica, Drożdżewski, et al. (2019). The two techniques are different in terms of weighting, for which we apply a ratio of 1:4 for GNSS and SLR NEQs, respectively, which means that we assume that SLR observations are four times less accurate than microwave phase observations (Bury et al., 2021). In all the cases, we estimate station coordinates, GNSS orbit parameters, ERPs, and, depending on the strategy, GCC (see Table 3). Co-location using SLR and GNSS observations demands homogeneous models as described in Table 1. We process different test cases, all of which are listed in Table 3 and the estimated parameters are listed in Table 2.

3. Results

We search for the best strategy for the co-location onboard GNSS satellites by analyzing the residuals from the Helmert transformation between particular solutions and between solutions and the a priori coordinates, by analyzing the formal errors of coordinates and the station coordinate repeatability. For the best strategies, we employ the space ties to retrieve the local ties and compare them with local ties obtained from the *in situ* measurements and values calculated using a priori coordinates. Moreover, we take a closer look at the handling of SLR range biases to check if the approach established by Appleby et al. (2016) developed for LAGEOS can be expanded and applied while combining SLR and GNSS data. Finally, we check the impact of the addition of SLR observations on the estimation of the global geodetic parameters.

3.1. Geodetic Datum Realization

We test a number of strategies in which we impose different constraints on GNSS and SLR networks. This allows us to develop the best strategy for the realization of the combined GNSS and SLR network and the evaluation of the strength of the linkage between the two techniques onboard GNSS satellites. We consider

Table 2
List of Estimated Parameters

Parameter	GNSS	SLR
Station coordinates	X, Y, Z for each GNSS and SLR station with NNR/NNT constraints for datum defining stations (depending on strategy–see Table 3)	
datum defining stations for NNR/NNT	GNSS stations for which residuals of the Helmert transformation do not exceed 1 cm for the horizontal and 3 cm for the vertical coordinates	Set of the SLRF2014 core stations reduced by stations showing systematic effects McDonald (7080), Changchun (7237), Wettzell (8834)
Pole coordinates	X pole, Y pole; two parameters per each component per day	
UT1-UTC	Initial value fixed to the a priori from IERS-14-C04, the drift of the UT1-UTC freely estimated (denoted as LoD)	
Geocenter coordinates	X, Y, Z per each day (depending on strategy)	
Orbital elements	GNSS orbit parameters: 6 Keplerian, 5 ECOM: D_0, Y_0, B_0, B_{1C}, B_{1S} + pseudo-stochastic orbit parameters in the radial, along-track, and cross-track directions every 12 h	
Troposphere	Site-specific zenith total delay (1 h), gradients (12 h)	-
Range Biases	-	Annual range biases calculated for each satellite-station pair; resubstituted and strongly constrained to a priori in the combined solution: (a) based solely on SLR observations to GNSS satellites, (b) considering the microwave GNSS observations, (c) and considering microwave GNSS observations and SLR observations to LAGEOS

three sets of sites, that is, GNSS, SLR, and combined SLR and GNSS networks. We then derive Helmert transformation parameters between each network for the different strategies. In Table 4 the mean and STD of the daily transformation values over the two years are given. Below, we show the key analyses, whereas the full set of figures illustrating Helmert transformation parameters is attached as Supporting Information S1. Note that in every scenario, all the GNSS and SLR stations are considered as a consistent set of stations forming one common network. However, the modification of the Bernese GNSS Software allows for imposing minimum constraints on the chosen subset of sites representing only one technique. As a result, even though we consider two sets of stations we cope with the same degree of freedom as it would be one network of sites, that is, three translations for each of the X, Y, and Z directions, three rotations, and one for the scale. Assuming that space ties did not provide sufficient connections between SLR and GNSS techniques, the SLR and GNSS networks would be fully independent and co-exist with separate origins, orientations, and scales in the combined solution. The strength of the connection can be thus evaluated by assessing the stability of the transformation parameters for each day.

The transformation parameters for the GNSS network are referred to the solution *M*1. At first, we calculate the solution *C*1, which is consistent with the solution *M*1 for GNSS, and considers the same constraining for the SLR network, that is, NNT + NNR for the SLR core stations (see Table 3). As a result, the Helmert transformation parameters between solutions *M*1 and *C*1 are nearly at a zero level for the GNSS network (see Table 4). The solution *C*1 was already proved to be sufficient for the precise Galileo orbit determination using combined GNSS and SLR observations (Bury et al., 2021). Concerning SLR station coordinates, the 1-day solution is insufficient to provide reliable station positions due to the low number of SLR observations. As a result, instead of comparing the solution *C*1 with the SLR-only solution, we relate the SLR station coordinates calculated using solution *C*1 to the a priori coordinates from the SLRF2014 as it comprises a long-term stable solution. Noteworthy, the realizations of the SLR frame in SLRF2014 and this solution are based on a different set of satellites. Moreover, due to a low number of SLR observations, the RMS of the transformation, that is, the measure of station agreement is at the level of 44 mm; hence the estimates of translation parameters which are at the level of 5.9 $\pm$ 7.8, 4.3 $\pm$ 5.6, and 6.3 $\pm$ 7.9 mm, for the X, Y, and Z component, respectively (see Table 4). The rotation between the two networks is below 0.1 μas for each of the X, Y, and Z-axes. Henceforth, the remaining transformation concerning the GNSS, SLR, and combined network will be referred to the solution *C*1.

At first, we tested how the constraints imposed on the GNSS network can realize the SLR network. The *G*1 approach is consistent in terms of imposing the minimum constraints with that proposed by Thaller

Table 3
List of Computation Strategies in Terms of the Constraints Imposed on the SLR and GNSS Networks and the Estimation of Geocenter Coordinates (GCC)

Solution	GNSS	SLR	GCC
*M*1	NNT/NNR	-	Yes
*C*1	NNT/NNR	NNT/NNR	Yes
*G*1	NNT/NNR	no constraints	Yes
*S*1	no constraints	NNT/NNR	Yes
*C*2	NNR	NNT	No
*C*3	NNR	NNR	No
*C*4	NNR/NNT	NNT	Yes
*C*5	NNR	NNT/NNR	Yes

et al. (2011) with the exception that Thaller et al. (2011) computed the stacked one-year solution, whereas the solution in this study is epoch-wise for each 1-day of the analyzed period. Concerning the GNSS network, the minimum constraints are the same as in the reference solution *C*1, therefore the transformation parameters are barely different. In *G*1 there are no constraints for the SLR network (see Table 3). Due to a relatively low number of SLR observations to GNSS satellites, both translation and rotation cannot reliably be transferred via GNSS satellites if no constraints are imposed on the SLR network. The SLR network is sparse and inhomogeneous as compared to the GNSS network, therefore during a single day, it provides a significantly smaller number of SLR observations as compared to the microwave ones. Therefore, the poorly realized SLR network influences the combined network, which is inconsistent in terms of the origin and orientation with the reference obtained from solution *C*1 (see Table 4). Despite that, the 3D SLR station coordinates repeatability computed using solution *G*1 is at an acceptable level, which is described below.

The solution *S*1 is complementary to the solution *G*1, as the minimum constraints are imposed on the SLR network and the GNSS network is free. However, imposing NNT and NNR constraints on a small set of SLR stations is insufficient for the determination of reliable combined solutions as the formal errors of the ERPs are at the level of over 80 mas. For a trustworthy solution, we expect formal errors of X-pole and Y-pole coordinates to be at the level of 0.015 mas; hence the solution *S*1 will not be considered in the following analyses.

In strategy *C*2, we impose the NNR constraint on the GNSS network and NNT for the SLR network. The GCC are not estimated. A lack of the estimation of the GCC is reasonable as the NNT constraint is not

Table 4
Helmert Transformation Parameters

Solutions		RMS [mm]	T_x [mm]	T_y [mm]	T_z [mm]	Scale [μm/km]	R_x [μas]	R_y [μas]	R_z [μas]
GNSS network									
*M*1	*C*1	0.3 ± 0.2	0.0 ± 0.0	0.0 ± 0.0	0.0 ± 0.0	0.0 ± 0.0	−0.1 ± 1.5	−0.2 ± 1.4	−0.1 ± 1.6
*C*1	*G*1	0.2 ± 0.2	0.0 ± 0.0	0.0 ± 0.0	0.0 ± 0.0	0.0 ± 0.0	−0.1 ± 1.5	−0.2 ± 1.4	−0.1 ± 1.6
*C*1	*C*2	0.2 ± 0.2	1.4 ± 4.6	−3.7 ± 5.9	2.8 ± 10.1	0.0 ± 0.0	0.4 ± 1.8	−0.1 ± 1.4	−0.5 ± 1.9
*C*1	*C*3	0.2 ± 0.2	1.6 ± 4.6	−3.7 ± 5.8	4.3 ± 10.6	0.0 ± 0.0	−0.2 ± 1.1	−0.0 ± 1.1	0.2 ± 1.2
*C*1	*C*4	0.1 ± 0.1	−0.0 ± 0.0	−0.0 ± 0.0	0.0 ± 0.0	0.0 ± 0.0	0.1 ± 1.4	−0.1 ± 1.3	−0.2 ± 1.6
*C*1	*C*5	0.2 ± 0.2	−13.0 ± 37.7	−6.0 ± 33.9	−6.9 ± 27.0	0.0 ± 0.0	−0.2 ± 1.2	−0.0 ± 1.1	0.2 ± 1.2
SLR network									
SLRF2014	*C*1	44.3 ± 45.1	5.9 ± 7.8	4.3 ± 5.6	6.3 ± 7.9	−3.7 ± 3.3	0.0 ± 0.8	0.1 ± 0.8	0.1 ± 0.8
*C*1	*G*1	7.4e2 ± 4.1e3	79.8 ± 2.2e3	−19.9 ± 1.5e3	32.0 ± 2.5e3	−6.9 ± 134.0	9.5e3± 2.8e5	1.1e3 ± 0.6e5	7.0e3 ± 3.0e5
*C*1	*C*2	55.8 ± 164.5	−1.9 ± 75.6	−0.4 ± 78.8	3.5 ± 60.4	−0.2 ± 7.8	248.7 ± 4.8e3	−208.9 ± 3.2e3	91.4 ± 5.9e3
*C*1	*C*3	53.0 ± 220.5	15.5 ± 38.8	2.7 ± 32.7	12.3 ± 29.2	−0.8 ± 8.1	0.1 ± 0.6	−0.0 ± 0.6	−0.1 ± 0.7
*C*1	*C*4	46.4 ± 157.8	−0.7 ± 58.8	0.0 ± 74.0	2.1 ± 47.4	−0.1 ± 7.2	172.0 ± 3.9e3	−120.4 ± 2.5e3	31.7 ± 5.0e3
*C*1	*C*5	53.5 ± 223.5	1.1 ± 9.5	1.0 ± 6.1	1.3 ± 15.3	−0.8 ± 8.2	0.1 ± 0.6	−0.0 ± 0.6	−0.1 ± 0.7
Combined SLR and GNSS network									
*C*1	*G*1	283.8 ± 1.6e9	16.7 ± 235.8	−0.2 ± 226.1	−2.7 ± 96.3	−0.1 ± 19.6	266.4 ± 1.1e4	53.3 ± 0.6e4	85.3 ± 1.8e4
*C*1	*C*2	20.5 ± 51.3	1.3 ± 4.4	−3.3 ± 5.4	2.6 ± 9.0	−0.0 ± 0.9	34.8 ± 337.3	−21.0 ± 263.6	−8.4 ± 294.8
*C*1	*C*3	18.1 ± 62.5	3.2 ± 6.2	−3.0 ± 6.4	5.3 ± 11.2	0.0 ± 0.9	11.9 ± 78.5	−17.2 ± 78.0	−5.2 ± 46.3
*C*1	*C*4	17.2 ± 48.5	0.1 ± 1.6	−0.1 ± 1.5	0.1 ± 1.7	−0.0 ± 0.9	25.4 ± 315.3	−15.0 ± 218.2	−6.3 ± 266.2
*C*1	*C*5	18.4 ± 63.5	−11.3 ± 33.3	−5.3 ± 30.3	−5.9 ± 23.9	0.0 ± 0.9	11.5 ± −80.3	−17.9 ± 79.1	5.4 ± 49.5

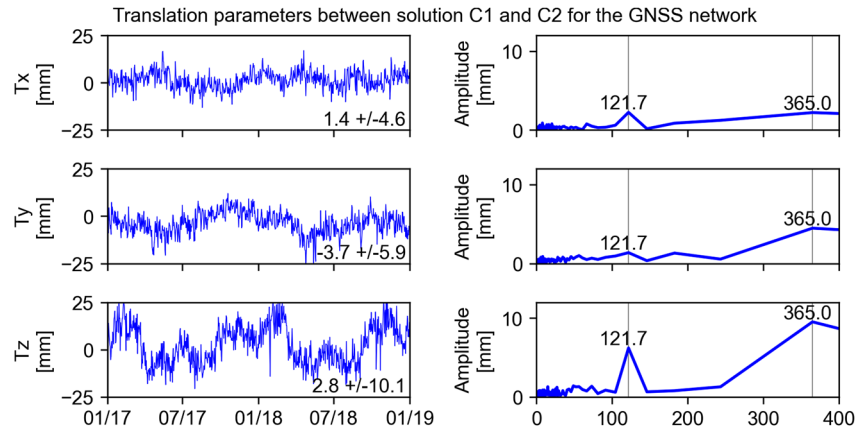

Figure 3. Time series (left) and amplitude spectra (right) of the translation parameters between GNSS stations calculated using solutions *C*1 and *C*2. Periods (right) are given in days.

imposed on the GNSS network dominating the solution. However, the geocenter motion, which has been absorbed by the GNSS stations in solution *C*2, is now reflected in the translation between solution *C*1 and *C*2. As a result, the translation parameters between the combined GNSS and SLR network of stations from solution *C*1 and *C*2 are at the level of 1.3 ± 4.4, -3.3 ± 5.4, and 2.6 ± 9.0, for the X, Y, and Z direction, respectively. With the amplitude of the annual signal at the level of 2.2, 4.5, and 9.5 for the X, Y, and Z components, respectively (see Figure 3), the translation parameters correspond to the signal of the GNSS-based geocenter motion calculated by Zajdel et al. (2021).

As the NNR constraint is imposed, we do not see any significant differences in the rotations between the GNSS network calculated using solutions *C*1 and *C*2. GNSS is a well-established technique for estimating the ERPs thanks to a dense, globally distributed network of GNSS tracking stations, good observation geometry, and continuous satellite tracking (Ray et al., 2017). However, when NNR is not imposed on the set of the SLR stations, the network orientation cannot be transferred from the GNSS network through the satellites onto the SLR network. The mean rotation parameters between solutions *C*1 and *C*2 for the combined solution might not be high but are unstable and noisy, that is, 34.8 ± 337.3, -21.0 ± 263.6, -8.4 ± 294.8 mm, for the X, Y, and Z component, respectively.

Strategy *C*3 is consistent with strategy *C*2 in terms of the GNSS network constraining. As a result, the transformation parameters between the GNSS network in solutions *C*3 and *C*1, and *C*2 and *C*1 are virtually the same. The main difference between solutions *C*3 and *C*2 is introduced to the SLR network constraining, that is, the NNT constraint is replaced by NNR. As a result, the orientation which could not be transferred via GNSS satellites to the SLR network is now constrained by the NNR constraint. Therefore, the rotation parameters between solution *C*3 and *C*1, are at zero levels for SLR and GNSS networks. As the NNT constraint is applied neither on the GNSS nor on the SLR network, the GCC signal has been revealed in both series of the translation parameters between solutions *C*1 and *C*3 for GNSS and SLR network, and as a consequence, also in the combined GNSS and SLR network.

Apart from the geocenter motion, another discrepancy between the reference *C*1 and the *C*3 solution occurs in the rotation between combined GNSS and SLR networks. Despite the NNR constraint imposed on the two networks separately, the combined network from the solution *C*3 is rotated w.r.t the combined network from the solution *C*1 by 11.9 ± 78.5, -17.2 ± 78.0, and -5.2 ± 46.3 μas around the X, Y, and Z-axis, respectively, which translates into 21, −30, and −9 mm projected to the equatorial plane. This discrepancy reveals the internal inconsistencies between SLR and GNSS a priori frames, which include differences in the network origin that cannot be absorbed by the GCC parameter. The RMS of transformation is at the level of 18.1 ± 62.5 mm, whereas the difference in the scale between solutions *C*1 and *C*3 is negligible.

In contrast to *C*2 and *C*3, we estimate the GCC in the test cases *C*4 and *C*5. The solution *C*4 treats the GNSS network in the same manner as the solution *C*1; hence the transformation parameters between the two solutions are at zero level for the GNSS network. As the rotation is not constrained for the SLR sites, the

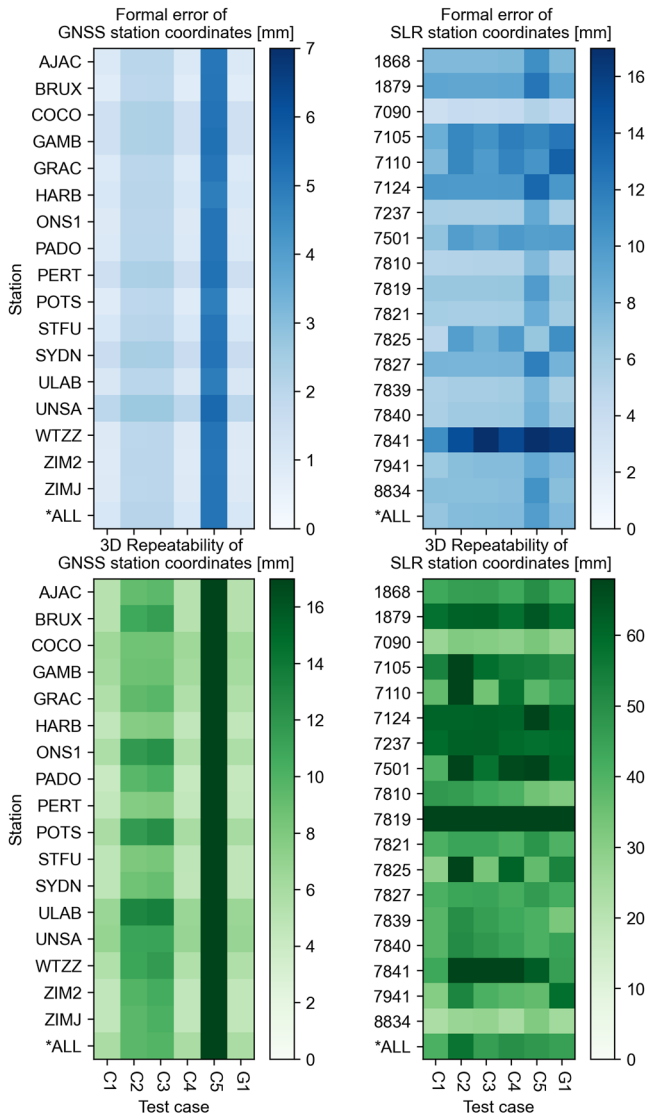

Figure 4. Formal error (top) and 3D station coordinate repeatability (bottom) for GNSS (left) and SLR stations (right) for each test case. *ALL denotes the median values for all the stations.

orientation of the SLR network cannot reliably be transferred via GNSS satellites, as it is in the case of solution *C*2. As a result, the transformation parameters between solutions *C*4 and *C*1 are similar to those from solutions *C*2 and *C*1, except for the geocenter motion whose signal is absorbed by the station coordinates when calculated using the solution *C*2, rather than in a separate parameter as it is in the case of solution *C*4. In solution *C*5, despite the GCC estimation, there is a spurious signal in the translation for the GNSS network between solutions *C*5 and *C*1. The GNSS network translation is free, but the GCC are estimated, which causes a partial rank defect of the GNSS network orientation at the level of 30 mm. However, the NNT and NNR constraints imposed on the SLR network in *C*5 seem to harm the GNSS network translation and GCC, which is described below.

To realize the combined GNSS and SLR network, solution *C*1 seems to be the most reliable as the NNT and NNR constraints imposed on the set of GNSS and SLR stations provide a reliable network orientation. The geocenter motion absorbed by a dedicated parameter (GCC) releases the origin of TRF from the systematic shift. The geocenter motion sensed by the GNSS satellites is perturbed by the non-conservative forces, such as direct solar radiation pressure. Moreover, the sensitivity of the GNSS pseudoranges to the geocenter recovery is limited, which is why the GNSS-based geocenter motion is sometimes called "apparent geocenter" (Ferland & Piraszewski, 2009). As a result, it is more reasonable to absorb the apparent geocenter motion by a separate parameter. If the GCC are not estimated, the most reliable solution, based on the Helmert transformation, is the solution *C*3, as the transformation parameters between solutions *C*1 and *C*3 are at the millimeter level.

3.2. Station Coordinate Quality

The minimum constraints control the geometry of the station network. We check if imposing the minimum constraints influences the quality of the determination of the station coordinates. We assess the formal errors of the estimated station coordinates to evaluate the solution precision. We also calculate the 3D station coordinate repeatability w.r.t the mean station coordinate estimates to provide information about the precision of the calculated coordinates.

Considering the GNSS stations, the high quality of the estimated coordinates results from a dense, globally distributed network of sites, and a huge number of collected observations. Figure 4 illustrates the formal error of the estimated 3D position and the 3D coordinate repeatability. The results from most of the GNSS stations are similar, with few exceptions, for example, for the ULAB station. As a result, the differences between the datum realization strategies are more pronounced in the global network transformation parameters than the differences resulting from the single stations.

The initial analysis of the formal error and station repeatability reveals the best way of imposing the minimum constraints on the network of the GNSS sites (see Figure 4). Both the analyses indicate the superiority of NNT and NNR constraints imposed simultaneously on the GNSS network. The median formal error for all the GNSS stations is at the level of 1.1, 1.1, and 1.1 mm, and the median 3D station coordinate repeatability equals 5.9, 5.9, and 5.8 mm for solutions *G*1, *C*4, and *C*1, respectively. Solutions *C*2 and *C*3 are characterized by a slightly worse quality, as the translation of the GNSS network is not constrained and the GCC are not estimated. As a result, the station position errors are amplified by geocenter motion signal which affects both the formal errors and the coordinate repeatability. The quality of the station coordinates might not considerably be inferior; yet it is twice as worse as compared to the solutions *G*1, *C*4, and *C*1, as

the formal error of the station coordinates is at the level of 2.1 and 2.1 mm, and the median repeatability of the calculated position equals 9.6, and 9.8 mm, for *C*2 and *C*3, respectively. As in the case of the datum realization, the quality of the estimated station coordinates using solution *C*5 is the worst. The lack of the NNT constraint and the estimated GCC deteriorate the solution as both, the formal error and the station coordinate repeatability, are over five times higher than in the case of solutions *G*1, *C*4, and *C*1.

The SLR network is inhomogeneous, for example, in terms of the equipment used at individual sites or the number of collected observations (Pearlman et al., 2019). Therefore, the diversity of the calculated coordinates for different stations can easily be seen (see Figure 4), apart from the differences in the quality of different test cases. This stems from the different quality and amount of data that are provided by the SLR stations. For the best-performing stations, for example, Yarragadee (7090), Zimmerwald (7810), Wettzell (7827 and 8834), or Matera (7941), the quality of the station coordinates is the highest regardless of the calculation strategy.

As in the case of the GNSS stations, the estimated SLR station coordinates using solution *C*5 are characterized by the highest formal error with the median value at the level of 9.7 mm and the highest 3D coordinate repeatability for 45% of stations. The second worst solution for the SLR stations is solution *C*2 in which only the NNT constraint was imposed on the SLR network. The worst values of the station coordinate repeatability were obtained for stations Greenbelt (7105), Monument Peak (7110), Mount Stromlo (7825), and Hartebeesthoek (7501) on which we impose the NNT constraint as they constitute the subset of the SLR core stations. In solution *C*2, station positions additionally absorb the geocenter motion, which indicates a spurious signal when calculated using GNSS satellites. A similar pattern is visible for the station positions calculated in solution *C*4 which treats the SLR network in the same manner as *C*2. Lower values of the coordinates repeatability in *C*4 result from the estimated GCC which absorbed the geocenter motion with the real geophysical and apparent signals. Nonetheless, when only the NNT constraint is applied on the SLR network, the station coordinates are not determined reliably as the median station repeatability is at the level of 56.9 and 50.0 mm for *C*2 and *C*4, respectively.

In Section 3.1, we demonstrated that the orientation of the SLR network cannot reliably be transferred via the GNSS satellites. As a result, in contrast to *C*2 and *C*4, for the core SLR sites in solution *C*3, we impose the NNR constraint. Such a treatment is also beneficial for the station coordinate repeatability, as the median value for all the stations is at the level of 45.9 mm. This is especially pronounced for the SLR core stations such as 7110 and 7825 for which the repeatability of the calculated coordinates using solution *C*3 is better by 50% and 44%, respectively, as compared to the solution *C*2.

Surprisingly, for 48% of SLR stations, the best repeatability of the calculated position is obtained for solution *G*1, which neglects to impose the minimum constraints on the SLR network. Although neither the origin nor the orientation of the network as a whole can be transferred via the GNSS satellites, the precision of the determined individual site positions is at the level of 47.6 mm and the median formal error is at the same level as for the other solutions. Therefore, we infer that the strength of the SLR-GNSS co-location onboard GNSS satellites is at the level of 40–50 mm in 1-day solutions.

Notwithstanding, taking into consideration of a reliable datum realization with high accuracy of the calculated station coordinates, the best results are obtained using solution *C*1. The median formal error and the station coordinate repeatability are at the level of ∼6.7 and 40.7 mm, respectively. The advantage of solution *C*1 is also visible in the case of single stations such as Potsdam (7841) and Mount Stromlo (7825) for which the solution *C*1 provides the best results compared to the other test cases.

3.3. Calculation of the Local Ties Using Co-Location Onboard GNSS

The realization of TRF demands coping with a proper linkage between individual space techniques. Such a connection is usually provided in the form of a so-called local tie, which is surveyed using ground observations collected with high-precision geodetic tools. However, such a process demands coping with uncertainties concerning the identification of the exact position in the sensor where the space observations are gathered w.r.t the reference points. Moreover, local tie measurements are being carried out occasionally. The inter-technique linkage can be transferred via satellites in the form of space ties, which is possible in

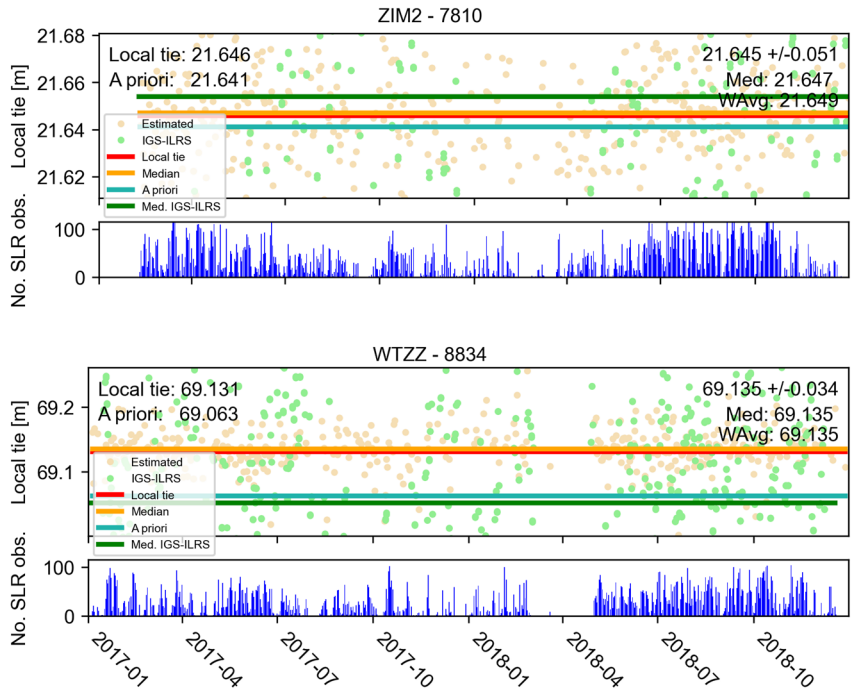

Figure 5. 3D local ties calculated using scenario *C*1 for GNSS-SLR co-located stations at Zimmerwald (top) and Wettzell (bottom) and the number of SLR observations as a function of time. Faint orange and green dots illustrate single solutions based on the co-location in space and single differences between the SLR and GNSS station positions from the official ILRS and IGS products, respectively. The red, orange, turquoise, and green lines denote the local tie measured *in situ*, the median value of the calculated local tie from the SLR-GNSS co-location in space, the distance between GNSS-SLR stations calculated using a priori coordinates from ITRF2014 and SLRF2014, and the median distance calculated using the coordinates from official IGS and ILRS products for the analyzed period, respectively. WAvg denotes weighted average (mean value) where the SLR station coordinate estimate formal errors constitute the weights.

terms of the GNSS and SLR techniques that are co-located on the majority of the navigation satellites and the global ties by co-sharing the common global geodetic parameters in the combined solution.

In this study, we use local ties only for the comparison, which means that the measured local ties do not contribute to the combined SLR-GNSS solution. Hence, we entirely rely on the connection onboard GNSS satellites. Figure 5 illustrates 3D space ties calculated using solution *C*1 (orange dots and lines) w.r.t the local ties measured on the ground (red line), and distances between SLR and GNSS stations calculated using (a) a priori coordinates from SLRF2014 and ITRF2014 (turquoise line), and (b) using coordinates provided by the ILRS and the IGS from the operational final products (green dots and line). The first and most important fact is a great agreement of the calculated space ties (orange line) with the distance obtained from the *in situ* measurements (red line). Without introducing any a priori information about the distance between SLR and GNSS stations based on the *in situ* measurements, we obtain the agreements of the 3D space ties at the level of ∼1 and 4 mm for Zimmerwald and Wettzell, respectively.

Second, imposing NNT and NNR constraints on the combined SLR and GNSS core stations does not tie the a posteriori station coordinates to the a priori positions. As a result, the calculated space ties do not depend on the a priori positions referred to the ITRF2014/SLRF2014, and the calculated station positions are realized by the GNSS and SLR observations obtained from the common network of GNSS and SLR stations estimated in the consistent processing. Additionally, the calculated coordinates are not consistent with the station positions calculated by the IGS and ILRS on the operational basis, which comprise fully independent solutions and two independent networks of SLR and GNSS stations. The discrepancy between GNSS and SLR stations from IGS and ILRS final product solutions and the calculated space ties is at the level of ∼83 and 7 mm for Wettzell and Zimmerwald, respectively. Therefore, to get the information about the distance between co-located SLR-GNSS stations which is consistent with the ground measurements information,

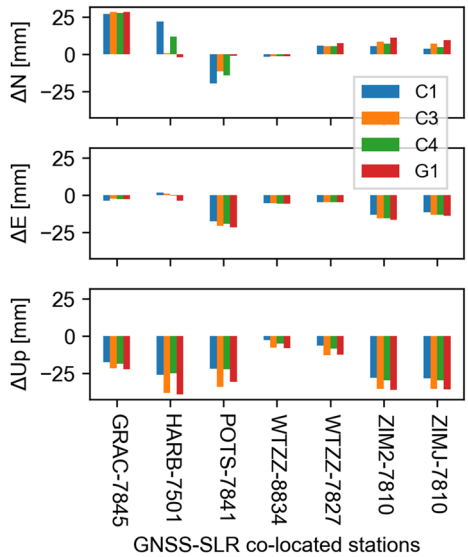

Figure 6. Differences between local ties calculated based on station coordinates determined from the GNSS-SLR co-location in space and using *in situ* local ties measurements decomposed into the North (N), East (E), and Up components for each GNSS-SLR pair for chosen solutions.

but is calculated using solely space technique observations, one has to conduct co-location onboard GNSS satellites.

Apart from the median value of the estimated local ties, we calculated the weighted mean of the estimated local tie values. As for the weights, we take the formal errors of the SLR station position estimates because the quality of the GNSS-SLR linkage seems to be directly subject to the quality of the SLR station coordinates. Unusually, for this study SLR site positions are calculated using SLR-to-GNSS observations, not based on the SLR-to-LAGEOS and ETALON observations. Additionally, the operational ILRS solution considers 7-day orbital arcs whereas in this study we calculate 1-day arcs for all the solutions. Despite all these, the weighted mean does not substantially diverge from the median statistic for Zimmerwald (2 mm) and Wettzell (0 mm), proving the SLR observations to GNSS satellites can contribute to the GNSS-SLR space ties calculation.

We also took a closer look at the number of SLR observations used for the local ties calculation. Over the analyzed period of two years, it was possible to determine space ties using GNSS-SLR co-location in over 58% and 66% cases for pairs WTZZ-8834 and ZIMJ-7810, respectively, which is remarkable when taking into account gaps in the SLR observations in the two cases. With the increase in the number of SLR observations, the calculated values of the local ties are gathered around the median value. The high efficiency of the space tie calculations can provide a close-to-continuous possibility of controlling the local tie values and can be carried out whenever the SLR and GNSS data are available. The standard deviations of the calculated local ties at Zimmerwald and Wettzell are 51 and 34 mm, respectively, which corresponds to the strength of the individual 1-day space tie connections provided for these stations. Moreover, the common processing of the GNSS and SLR observations makes the realization of the TRF independent of *in situ* measurements. Additionally, local ties calculated using space techniques can contribute to the realization of TRF as an independent observation with full variance-covariance information as provided by the geometry and quality of observations.

The 3D space ties indicate how well we can recover the absolute distance between the co-located GNSS and SLR stations. However, it lacks information about the orientation of the linkage vector. As a result, we decomposed the space ties into the North, East, and Up components to check how well the co-location onboard GNSS satellites transfer the orientation of GNSS and SLR stations. Figure 6 illustrates the agreement of the calculated space ties using co-location in space with the measured *in situ* linkage vectors for chosen solutions. Most of the SLR stations are co-located with GPS receivers, however, only some of them are co-located with GNSS receivers tracking Galileo and GLONASS observations or local tie measurements were not surveyed for these new GNSS antennae with the possibility of collecting Galileo data. Therefore, the number of SLR-Galileo/GLONASS local ties is limited.

The solution in which we do not impose the minimum constraints on the SLR network (*G*1) provides the local ties values at a similar level to the other solutions (see Figure 6). This means that although the orientation of the SLR network in *G*1 is ill-defined from the results of the Helmert transformation, the orientation provided by the space tie is correct, and in some cases (North component of POTS-7841 and WTZZ-7827) even better than for the solutions which impose the minimum constraints to both networks. However, this is only valid when a sufficient number of SLR observations to GNSS satellites is provided. Although solution *C*3 indicated relatively low values of the formal error for the SLR position estimates, the agreement with the measured local ties is not as good as in the case of other solutions. For pairs HARB-7501 and POTS-7841, we notice differences between space ties calculated using different solutions. For the North component of HARB-7501 and East and Up components of POTS-7841 solutions, *C*1 and *C*4 provide the best agreement with the *in situ* measurements.

The solution *C*1 indicates the highest consistency with the *in situ* measurements for all components of both stations Wettzell and Zimmerwald connected via space ties. In the case of Wettzell, local ties are calculated

Table 5
Characteristic of Solutions With the Experimental Approaches to RBs

	NEQs			Coordinates and velocities	
Applied to solution	SLR-to-GNSS	SLR-to-LAGEOS	GNSS	GNSS network	SLR network
*C*1	+	−	−	−	Fixed
*C*1*G*	+	−	+	Estimated[a]	Estimated[a]
*C*1*L*	+	+	+	Estimated[a]	Estimated[a]

[a]NNT + NNR imposed on the core stations, the remaining station positions estimated.

and measured between the GNSS station (WTZZ) and two SLR stations 8834 and 7827. The East and Up components are consistent for the two station pairs, however, the North component indicates a positive discrepancy between calculated and measured local tie for the station 8834, and negative for 7827, which may result from differences between the position accuracy of the two SLR sites. In the case of Zimmerwald, two ties are calculated w.r.t the same SLR station and two GNSS stations. With no difference in the GNSS stations and presumably the same accuracy of the local tie measurements, the discrepancies between measured and calculated linkage are almost the same for the two cases.

For the pair GRAC-7845 in Grasse, the discrepancies between calculated and measured ties are the highest and reach the level of ∼−27, −21, and −18 mm, for the North, East, and Up components, respectively. This is due to the lowest number of SLR observations provided by station 7845, that is, 1730, when compared to 17,207 observations provided by station Wettzell (8834), during the whole analyzed period.

Considering all, the obtained results show that co-location onboard GNSS satellites is possible and the accuracy of the linkage between the best-performing pairs of GNSS and SLR stations is, in the worst case, at the level of 14 mm for the horizontal component of the local tie in Zimmerwald and 29 mm for the Up component for Wettzell.

3.4. Handling of SLR Range Biases

The quality of the SLR station coordinates in the combined solution is more vulnerable to systematic errors than the GNSS position estimates. First of all, the number of SLR observations is significantly lower than in the case of GNSS satellites. Second, the official SLR station coordinates are determined using SLR observations to the spherical, geodetic satellites such as LAGEOS and Etalon. Moreover, the SLR site coordinates are determined using 7-day orbital arcs whereas in this study we consider 1-day combined solutions. All these limitations force us to revise the methodology of the processing of the SLR observations to the GNSS satellites. One of the crucial aspects of SLR data processing is the handling of the SLR RBs. Due to the diversity in technical solutions used by almost every single station and their operational performance, we have to calculate the annual average SLR RBs for each satellite-station pair using only SLR observations to GNSS satellites. We calculate the annual mean SLR range biases with fixed to a priori station positions and GNSS orbits consistent with Bury et al. (2020). The RBs calculated using the basic approach are used in all the solutions listed in Table 3. Although the information provided by the SLR observations to GNSS satellites seems to be the best source about the connection between the SLR station detector and the LRA mounted on GNSS satellites, in some cases the number of observations is insufficient for resolving systematic errors from the side of the SLR station and estimate reliable RBs when using only SLR data to GNSS.

Therefore, we provide two additional tests for the SLR RBs, that is, (1) with the contribution of the microwave-GNSS observations and (2) with the contribution of GNSS observations and SLR observations to LAGEOS (see Table 5). The LAGEOS-based SLR station coordinates in (2) might be beneficial for stabilizing the SLR site position estimates and, therefore, the estimated values of the RBs. Moreover, the GNSS observations in (1) and (2) might also stabilize the solutions with a vast number of GNSS observations even though they are independent of SLR measurements. To consider different types of observations, we stack for the test (1) SLR-to-GNSS and microwave-GNSS NEQs, and in the test (2) additionally the SLR-to-LAGEOS NEQs (Figure 7). SLR-to-GNSS and GNSS NEQs are introduced in Section 2, whereas the SLR-to-LAGEOS NEQs introduced here include the geodetic parameters together with SLR station coordinates and orbits calculated using SLR observations to LAGEOS satellites. As in the case of the basic approach to RBs, in tests (1) and (2) we compute one stacked solutions from which we obtain mean values of RBs for each satellite-station pairs.

For the estimation of the experimental SLR RBs, we stack the two years of the 1-day (1) SLR-to-GNSS, GNSS, and (2) additionally, SLR-to-LAGEOS NEQs. In the two-year stacked solutions, we estimate GNSS

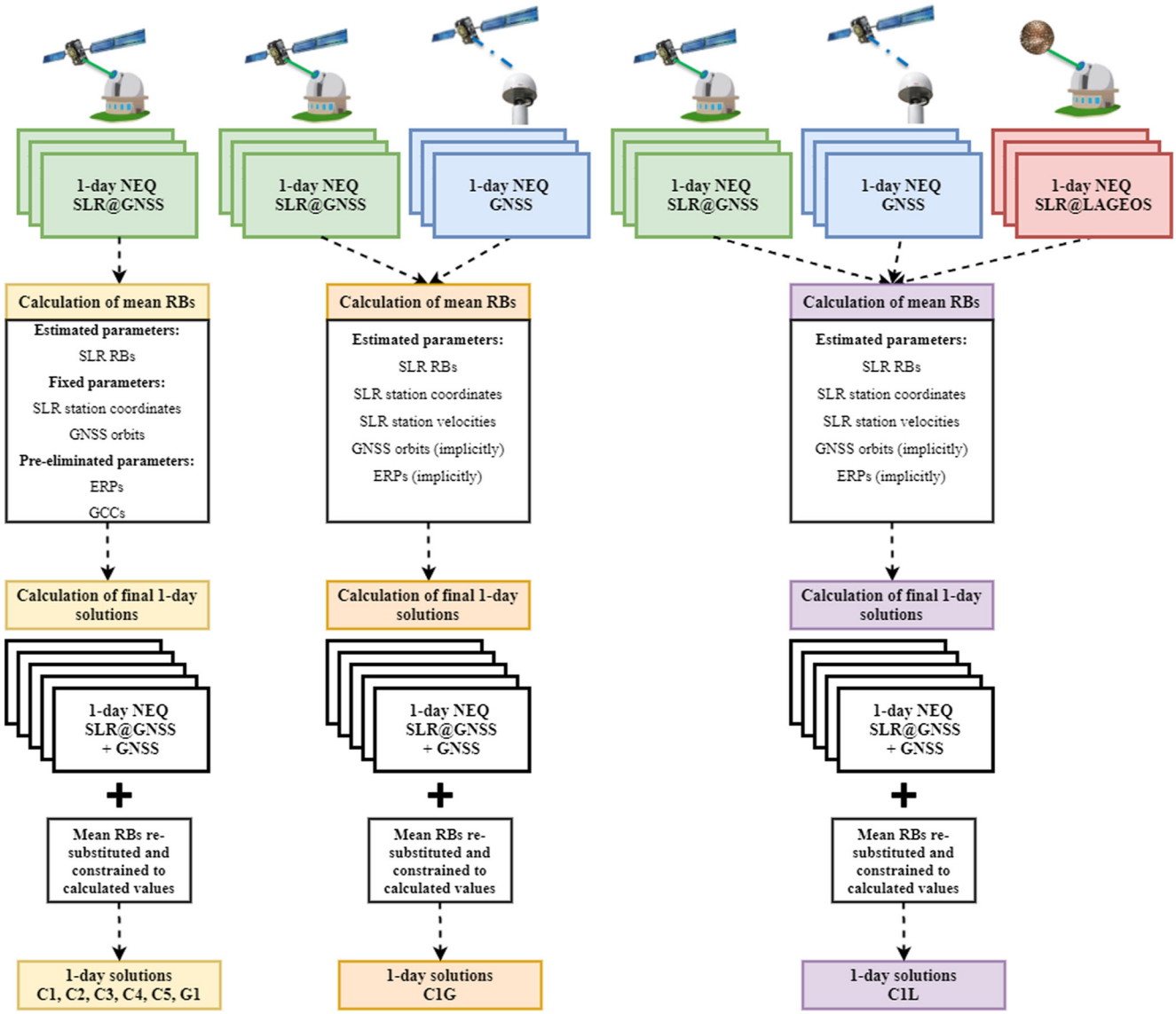

Figure 7. Scheme for the SLR RBs calculation and application in the final combined GNSS and SLR solutions.

and SLR station coordinates and velocities with NNT + NNR constraint imposed consistently with the solution *C*1, ERPs (implicitly), GNSS orbit parameters (implicitly), and SLR RBs. In the final processing, we re-substitute the newly calculated RB values as a priori and strongly constrain the estimates to their initial values. The solutions with the new values of SLR RBs are denoted as (1) *C*1*G* and (2) *C*1*L*. Noteworthy, for the epoch-wise processing of the 1-day solution *C*1*L* in which we estimate all the global geodetic parameters, GNSS orbits, and station coordinates we do not use the observations to the LAGEOS satellites. Thus, the LAGEOS observations are used only for the bias calibration of SLR observations to GNSS satellites.

Figure 8 depicts the RBs values used in the solution *C*1 and *C*1*L*. Considering the contribution of only SLR observations to the GNSS satellites, the SLR RBs depend mainly on the type of detector installed at the SLR station. Among the used detectors we can distinguish single- (CSPAD, SPAD) and multi-photon (PMT, MCP) detectors (Wilkinson et al., 2019). Different types of detectors imply different values of a so-called SLR signature effect (Otsubo et al., 2001). In general, stations equipped with multi-photon detectors are more vulnerable to the SLR signature effect as the detectors are not able to register a full range of returning photons. This transfers into median negative values of the SLR RBs for all GNSS satellites, for example, for Yarragadee (7090, −4.0 mm), Monument Peak (7110, −0.2 mm), Matera (7941, −2.8 mm), Wettzell

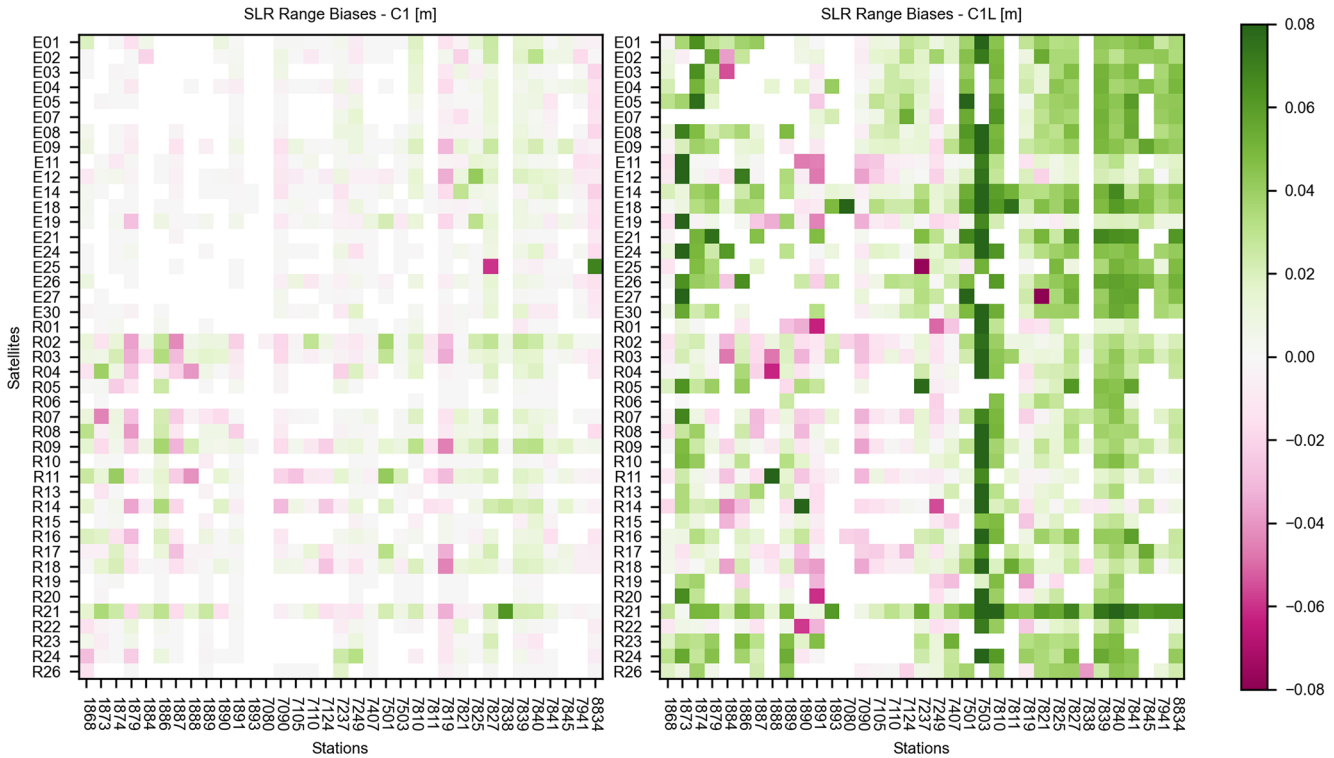

Figure 8. Annual mean SLR range biases for each GNSS satellite-SLR station pair estimated for the solution *C*1 (left) and *C*1*L* (right). Satellites are expressed with their PRNs. All values are given in meters.

(8834, −8.6 mm), and the Russian stations which track mainly the GLONASS satellites, that is, Altay (1879, −7.9 mm), and Baikonur (1887, −11.1 mm).

Let us now check how the addition of the microwave-GNSS and SLR-to-LAGEOS observations influences the estimated RBs. The introduction of the GNSS and SLR-to-LAGEOS observations increases the RBs values. This indicates that through the space ties the GNSS observations changed the RB values and the SLR observations to LAGEOS satellites stabilized the RBs compared to the solution *C*1. The addition of the SLR-to-LAGEOS observations does not directly impact the SLR-to-GNSS observations; however, it stabilizes the SLR station coordinates, which in the basic approach for RBs handling, rely solely on the SLR-to-GNSS data. In RBs calculated with the impact of the SLR-to-LAGEOS observations, the photon detector-dependence is increased, especially for stations Wettzell (8834) and Matera (7941) for which now the median RBs are at the level of 32.8 and 29.2 mm, respectively. In general, the RBs values in *C*1*L* are higher than those in solution *C*1. However, they are hardly comparable as the RBs from solution *C*1*L* might have absorbed not only the SLR-related errors but also the deficiencies in the modeling of the GNSS observations. The SLR RBs in solution *C*1*G* (not shown here) assume even higher values than those from solution *C*1*L* and therefore seem to be dominated by the vast number of GNSS observations. Moreover, all the RB values are positive, which indicates that the SLR-related artifacts might have been covered by the impact of a vast number of GNSS observations which reduce the influence of the SLR observations to GNSS satellites.

Nevertheless, at first sight, the absolute value of the RBs does not indicate which of the three solutions is the best. To find the best strategy, we compare the calculated local ties with the measured on ground linkage vectors. Figure 9 illustrates the differences between the calculated and measured *in situ* local ties used in solutions *C*1, *C*1*L*, and *C*1*G*. The *C*1 solution has been further improved with the new values of the SLR RBs from solution *C*1*L* as the differences between calculated and measured local ties have been significantly diminished almost for all the sites. The most pronounced differences are visible for the Zimmerwald, especially for the Up component of both local ties, as differences between calculated and measured local ties diminish from −28.6 to 0.7 mm for the pair ZIM2-7810. The horizontal components became more consistent as well, that is, the difference in the East component diminishes from −13.7 to 7.7 mm. The

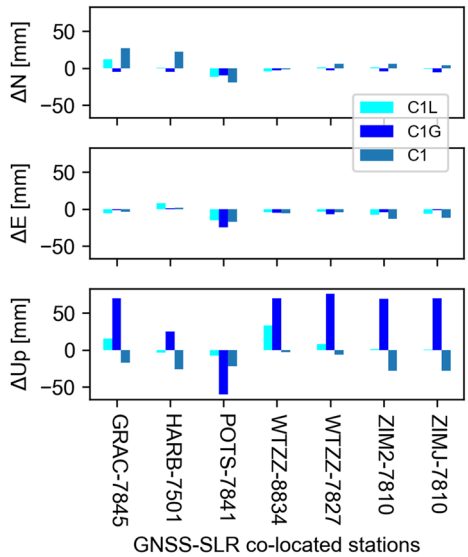

Figure 9. Difference between local ties calculated using co-location in space from *C*1, *C*1*L,* and *C*1*G* solutions and local ties based on *in situ* measurements decomposed into the North (N), East (E), and Up components for each GNSS-SLR station pair.

consistency of the Up component is improved also for pairs POTS-7841 (from −16.0 to −5.7 mm) and HARB-7501 (from 26.8 to 7.9 mm) or is at the same level but with a different sign for WTZZ-7827 (from −6.4 to 7.7 mm) and GRAC-7845 (−16.8 to 18.1 mm). The results indicate that the calculated Up component has been shifted upwards in most cases, diminishing the inconsistency of the calculated linkage with the measured *in situ* distance.

The only deterioration of the consistency is noticed for the pair WTZZ-8834 for which the consistency for the Up component is significantly deteriorated (from −3.0 to 32.9 mm). Although this seems to be a problem caused by the solution, during the analysis period, that is, 2017.0–2019.0, station 8834 must have suffered from some technical issue as the SLR residuals to microwave orbits indicated an offset at the level of −23.8 ± 25.8 mm as compared to 7.6 ± 27.1 for station 7827 (Zajdel et al., 2017). The improvement of the consistency of the Up component can be expected when the methodology of handling the range biases is improved as it directly impacts the station height.

The deterioration of the consistency between calculated and measured local ties in solution *C*1*G* confirms that the anomalously high values of the SLR RBs are erroneously dominated by the GNSS technique. Although the consistency is at a similar level as in solutions *C*1 and *C*1*L* for the horizontal, the Up component significantly deteriorates for co-located stations in Wettzell and Zimmerwald. As a result, the SLR RBs from the solution *C*1*L* are superior to those obtained based solely on the SLR solution, which neglects the LAGEOS satellites. The horizontal consistency of the stations has been improved, as well. In the case of Wettzell and Zimmerwald, it was already at 0.5–2.2 mm level. However, the improvement is more pronounced for pairs POTS-7841 (from 28.9 to 22.8 mm) and HARB-7501 (from 19.9 to 7.0 mm) for the horizontal components.

Table 6 summarizes the performance in calculation of the local ties based on solutions *C*1 and *C*1*L*. The calculated ties are compared with the distances calculated using (1) a priori SLR and GNSS station positions from SLRF2014 and ITRF2014, respectively, and (2) using the coordinates from the final products of the ILRS and IGS. All values in Table 6 are referred to 3D distance calculated concerning median values for each North, East, and Up components. In both *C*1 and *C*1*L* cases, the obtained local ties are consistent with ground measurements, which means that the calculated values are not artificially tied to the a priori reference frame, that is, ITRF2014 and SLRF2014. Moreover, the distance between calculated coordinates from the official final ILRS and IGS products is neither consistent with the distance calculated from a priori coordinates nor with the calculated and measured local ties. As a result, despite the connection with the a priori reference frames, the solutions of the ILRS and IGS are not consistent in terms of the co-located station coordinates. This brings us to the conclusion that using co-location onboard a satellite in space constitutes a consistent manner for the determination of the co-located station positions and might be treated with similar importance as the *in situ* ground measurements in terms of accuracy. When decomposed into

Table 6
3D Absolute Differences Concerning the Local Tie Orientation in Space, That Is, Calculated Distance Based on Median Values for North, East, and Up Component Between Calculated Local Ties Using Solutions C1 and C1L w.r.t Ground Measured (Local Tie), the Distance Between SLR and GNSS Station Calculated Using a Priori Coordinates Expressed in SLRF2014 and ITRF2014 and Final ILRS and IGS Products

	GRAC-7845		HARB-7501		POTS-7841		WTZZ-8834		WTZZ-7827		ZIM2-7810		ZIMJ-7810	
	*C*1	*C*1*L*	*C*1	*C*1*L*	*C*1	*C*1*L*	*C*1	*C*1*L*	*C*1	*C*1*L*	*C*1	*C*1*L*	*C*1	*C*1*L*
w.r.t Local tie	32.6	20.1	34.1	8.6	34.0	20.5	6.4	33.3	9.7	8.7	31.5	7.8	30.9	6.2
ITRF2014-SLRF2014	119.2	126.8	60.3	34.4	21.4	10.4	133.7	133.8	137.5	136.8	26.8	5.9	129.1	125.6
Final ILRS – Final IGS	164.5	153.2	212.2	192.4	99.4	103.5	113.0	111.4	61.9	56.0	103.5	95.0	104.5	96.0

Note. All values are given in millimeters.

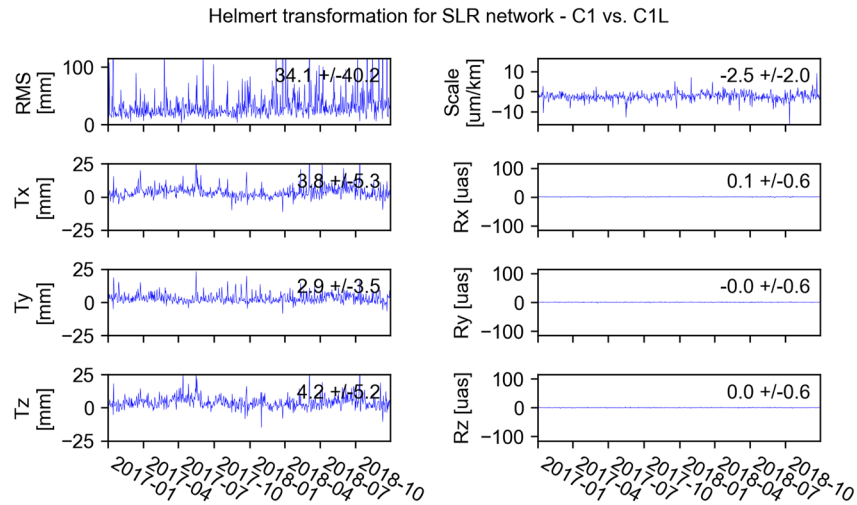

Figure 10. Helmert transformation parameters between SLR network calculated using solutions *C*1 and *C*1*L*.

the North, East, and Up components, solution *C*1*L* indicates the highest consistency with the *in situ* measured for the height component of the local tie. In terms of the horizontal coordinates, the quality of the connection is similar for *C*1 and *C*1*L* (see Figure 9). In all the cases, apart from Wettzell WTZZ-7827 stations' pairs, the solution *C*1*L* indicates the improved consistency with the ground measured local ties. The median improvement w.r.t the solution *C*1 is at the level of 69%, mostly owing to the improved Up component of local ties (see Figure 9).

Figure 10 shows Helmert transformation parameters between SLR networks derived using solutions *C*1 and *C*1*L*. The datum in the two solutions is realized in the same manner, that is, the NNT + NNR constraints are applied to the same set of SLR core stations. As a result, the transformation parameters indicate only the impact of the updated SLR RBs. Noteworthy, the two SLR datum definitions are based solely on the site position estimates using GNSS and SLR-to-GNSS observations. The modification of the SLR RBs does not impact the network orientation, as the SLR RBs are direct corrections to range measurements, which mostly influence the estimated height components of SLR station coordinates. The differences in station coordinates are reflected in the RMS of transformation parameters. The translations are at the level of 3.8 ± 5.3, 2.9 ± 3.5, 4.2 ± 5.2 mm for the X, Y, and Z components, respectively (Figure 10). The shift between the two networks is revealed not only in the translation parameters but also in the geocenter motion described in the following section. The important aspect by the definition of the combined datum is the global scale parameter. The current realization of scale in the ITRF2014 realized based on SLR and VLBI techniques suffers from the inconsistency at the level of 6.4 mm at the equator. The difference in scale between SLR networks from solutions *C*1 and *C*1*L* is at the level of -2.5 ± 2.0 mm/km, translating into 15.9 mm at the equator. In the *C*1 solution, the scale of the reference frame embedded in RBs is provided by the GNSS satellites and GNSS antenna calibrations, whereas in *C*1*L*, the scale embedded in RBs is provided by LAGEOS. Moreover, in *C*1, the RBs are calculated only based on SLR observations to GNSS satellites by a limited number of SLR sites when compared to the number of stations tracking LAGEOS satellites. Therefore the scale difference might result from different number and distribution of SLR sites in the two solutions. Noteworthy, both solutions are based on 1-day solutions which might be insufficient in terms of the scale parameter determination when compared to the standard 7-day solutions provided by ILRS. This analysis does not tell which of the two solutions is better; however, based on the analysis of the calculated space ties and the GCC, the solution *C*1*L* seems to be more consistent with the *in situ* measurements and the GNSS technique. Nevertheless, we infer that different handling of SLR RBs leads to different realizations of the TRF origin and scale.

Figure 11 illustrates the local tie for the pair WTZZ-7827 decomposed into the North, East, and Up components. The calculated space tie using solution *C*1*L* indicates an improvement of the consistency with the measured tie between SLR and GNSS stations, that is, the differences between the two vectors are at the

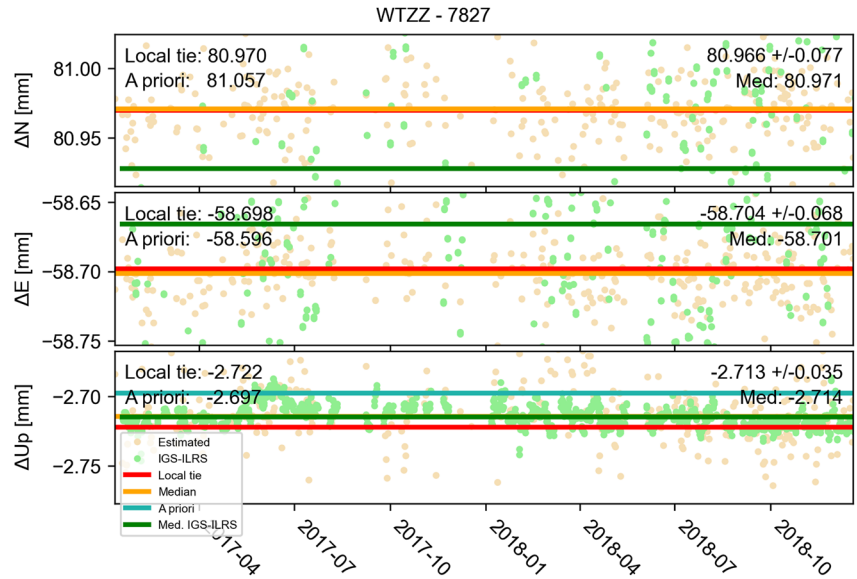

Figure 11. Local ties for WTZZ-7827 decomposed into the North, East, and Up, component from *C*1*L* solution. The nomenclature of the figure is consistent with Figure 5.

level of 1, 3, and 8 mm for the North, East, and Up components, respectively. The STD of the calculated space ties is diminished as well when compared to the solution *C*1, that is, from 80 to 77 mm, from 72 to 68 mm, and 39 to 35 mm for the North, East, and Up components, respectively. As a result, the application of the SLR RBs which consider the impact of the LAGEOS solution improves not only the reconstruction of the Up component of the local ties but also diminishes the STD for the horizontal component improving the consistency with the linkage vectors measured *in situ*. We tested also different approaches to the determination of station-specific RBs, for instance, the determination of RBs together with SLR station coordinate corrections and velocity corrections w.r.t. SLRF2014 based on SLR-to-GNSS NEQs and GNSS NEQs, for example, *C*1*G*. However, these approaches turned out to provide worse results and large-size TRF scale issues than *C*1, especially to *C*1*L*.

3.5. Impact of Combined Solutions on the Global Geodetic Parameters

Lastly, we check the impact of the combined GNSS + SLR solution on the global geometric parameters, that is, GCC and ERPs. The geocenter motion signal calculated using GNSS observations is dominated by spurious satellite-related artifacts resulting from for example, the deficiencies in the modeling of the direct solar radiation pressure (Meindl et al., 2013; Zajdel et al., 2021). Therefore, the apparent GCC calculated using GNSS observations do not exclusively carry the geophysical information as in the SLR technique when observing spherical geodetic satellites (Wu et al., 2012). Männel and Rothacher (2017) found that the combination of the ground-based observations with the GNSS observations to low earth orbiters (LEO) improves the formal error of the GCC by approximately 20%. We check whether the addition of the SLR observations to GNSS satellites impacts the calculated GCC and if so, we analyze which approach of the GNSS and SLR network constraining influences the geocenter motion signal.

The GCC obtained from *C*5 is erroneous with the STD of differences w.r.t GCC from solution *M*1 at the level of over 30 mm, which is similar to the quality of the station coordinates from *C*5. Apart from that, the course of the time series of GCC decomposed into the X, Y, and Z components are similar for all the remaining solutions. Figure 12 depicts the differences between GCC calculated using the microwave-based solution *M*1 and consecutive combined solutions *C*1*L*, *C*1, *C*4, and *G*1. Table 7 contains the characteristics of the GCC calculated using strategy *M*1 and the differences between GCC from *M*1 and other combined GNSS + SLR strategies. The GGC calculated using strategy *M*1 are consistent with the geocenter motion signal calculated for the multi-GNSS solution based on GPS, GLONASS, and Galileo satellites which were discussed by Zajdel et al. (2021). The highest consistency between the reference solution *M*1 is indicated

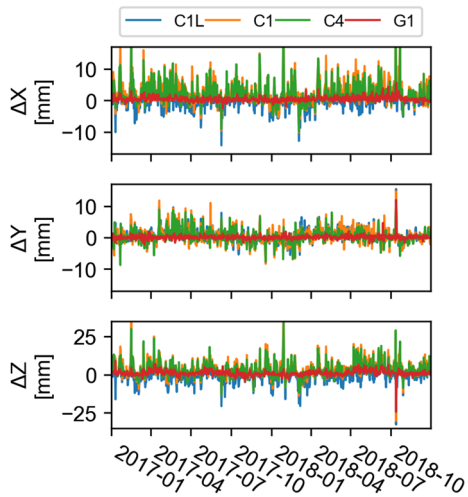

Figure 12. Difference between GCC calculated using solutions *M*1 and solutions *C*1*L*, *C*1, *C*4, and *G*1.

for the strategy *G*1 in which the SLR network is not constrained. As a result, the center of the combined GNSS + SLR network is tied to the GNSS center-of-network, that is, to the solution *M*1, consistent with the results presented by Thaller et al. (2014). The STD of horizontal components of GCC is at a zero level, and for the Z-component of the GCC, the STD is lower by −0.50 mm for *G*1 as compared to *M*1. The GCC obtained using solution *C*1*G* are consistent with those from solutions *M*1 and *G*1 which indicates that the solution *C*1*G* is dominated by the GNSS observations. Despite a spurious impact on the determined Up component of local ties, the GCC are determined consistently with GNSS-only solution with a slightly diminished offset by −0.06, −0.21, and −0.50 mm for the X, Y, and Z component, respectively. The solution C1L also is consistent with the GCC from the solution *M*1, and in the case of the Z-component of GCC, the offset is diminished by −0.6 mm. This results from a better quality of the SLR RBs determination when incorporating LAGEOS satellites for RB determination, and therefore, better realized TRF. Finally, in the solution *C*1*L,* the amplitude of the 1/3rd of the draconitic period is diminished by 17% compared to the solution *M*1 (not shown here).

Large differences are visible for the combined solution in which we impose the network constraining on both GNSS and SLR networks. However, in the case of solutions *C*1 and *C*4, the offset of the X- and Z-component of the GCC has been increased by 2.60 (1.92) and 3.69 (2.79) mm for solutions *C*1 (*C*4), respectively. Solutions *C*1 and *C*4 are consistent in terms of the GNSS network constraining. The only difference is the fact that for the SLR network in *C*1 we impose NNT + NNR, and in *C*4, only NNT. The fully constrained SLR network makes the GCC noisier, that is, in *C*1, the STD increases by 1.18 and 0.77 mm for GCC-X and GCC-Z, respectively.

The time series of GCC calculated using combined solutions are barely different from that obtained in solution *M*1. The most consistent GCC are obtained from the solution *G*1 in which the SLR network is not constrained. The other combined solutions indicate little differences when compared to the solution *M*1, which indicates that the selection of the space geodetic technique does not matter, whereas of crucial importance are the satellites based on which the GCC estimates are delivered. As a result, to obtain more reliable GCC, it is critical to address the issue of proper GNSS orbit modeling.

Concerning determined ERPs, they consist of the X-pole and Y-pole coordinates (polar motion, PM), rates of X- and Y-pole coordinates, UT1-UTC, and the rate of UT1-UTC, that is, the length-of-day (LoD). The GNSS constitutes the major technique for the recovery of reliable ERPs due to continuously transmitted navigation signals, a globally distributed network of GNSS receivers, and broad spectra of navigation satellites

Table 7
Offset and STD of the GCC Time Series Calculated Using Solution M1 Compared to a Priori IERS-C04-14 Values and Differences in Offsets and STDs of GCC Calculated Using Different Combined GNSS + SLR Solutions w.r.t the Solution M1

	X		Y		Z	
	Offset [mm]	STD [mm]	Offset [mm]	STD [mm]	Offset [mm]	STD [mm]
*M*1w.r.t IERS-C04-14	1.12	4.59	−3.79	5.87	3.37	11.15
Δ w.r.t *M*1						
*C*1*L*	0.10	0.59	0.62	−0.40	−0.61	0.45
*C*1*G*	−0.06	0.90	−0.21	−0.41	−0.50	1.43
*C*1	2.60	1.18	0.61	−0.26	3.69	0.77
*C*4	1.92	0.96	0.34	−0.20	2.79	0.46
*C*5	13.30	32.96	6.04	27.35	7.80	18.10
*G*1	0.43	0.04	0.08	−0.01	0.92	−0.49

Table 8
Offsets and STDs of the PM and LoD Calculated Using Solution M1 and Differences in Offset and STD of PM Calculated Using Combined GNSS + SLR Solutions w.r.t the Solution M1

	X-pole		Y-pole		LoD	
	Offset [μas]	STD [μas]	Offset [μas]	STD [μas]	Offset [μs/day]	STD [μs/day]
*M*1	31.20	60.70	−28.09	50.55	12.92	42.06
Δ w.r.t *M*1						
*C*1*L*	0.34	−0.56	0.47	−0.72	−1.92	−0.17
*C*1*G*	0.56	−0.72	−0.20	−0.27	−0.40	0.16
*C*1	−0.63	−0.03	0.21	−0.18	−3.45	−0.26
*C*2	0.62	−0.09	1.28	−0.06	−3.57	−0.17
*C*3	0.22	−0.22	−0.24	−0.05	−2.97	−0.25
*C*4	−0.70	−0.22	0.58	0.25	−3.28	−0.27
*C*5	0.22	−0.19	−0.12	0.02	−2.98	−0.26
*G*1	−0.19	0.11	0.00	−0.05	−2.99	−0.28

which are included within the emerging multi-GNSS constellations (Ray et al., 2017). As a result, we do not expect a significant impact of the combination of the GNSS observations with the range measurements to the GNSS satellites. Table 8 contains statistics for PM calculated using the solution *M*1 w.r.t. the a priori IERS-C04-14 values. Solution *M*1 can be treated as a reference, as it is computed based on solely microwave-GNSS data. Therefore in Table 8, the results of PM calculated using the remaining strategies considering combined SLR + GNSS observations are referred to the solution *M*1. All the calculations of X- and Y-pole are referred to the middle of the arc, that is, to hour 12. Finally, in Table 8 we collect the LoD statistics, considering the change value of UT1-UTC over one day, as the initial value is fixed to the a priori values.

The combination of the GNSS observations with the SLR observations to GNSS satellites does not significantly change the PM no matter of the SLR network constraining. The course of the PM corrections in all the solutions is nearly the same for both X-pole and Y-pole (not shown here). The absolute difference between offset for the solution *M1* and combined solutions is not higher than 0.70 and 1.28 μas for X-, and Y-pole, respectively. Similarly, for STD, the discrepancies between the GNSS-only and the combined SLR + GNSS are below the level of 0.72 μas, which can be classified as numerical errors rather than the impact of the addition of the SLR measurements.

The impact of the SLR observations in the combined solutions is most pronounced for the LoD. First, for all the combined solutions, there is an improvement of the determined LoD as the offset is diminished by up to −3.57 μs/day for solution *C*2 compared to solution *M*1 (Table 8). On average, for the combined solutions, the offset of LoD is diminished by −3.00 μs/day as compared to the microwave test case. The precision of LoD is improved as well, as the STD of determined LoD is lower on average by −0.24 μs/day for the combined solutions when compared to the strategy *M*1. The smallest improvement is noted for the solution with the updated RBs, that is, *C*1*G* for which the offset and STD are improved by −0.92, and −0.17 μs/day, respectively, as compared to solution *M*1. In the case of solution *C*1*G,* an offset is improved by −0.40 μs/day, however, the STD is increased by 0.16 μs/day. As a result, the GNSS microwave observations which are considered in the calculation of RBs in *C*1*L* and *C*1*G* seem to have a significant impact on the determined LoD parameter making the solutions *C*1*L* and *C*1*G* more consistent with the solution *M*1 than other combined SLR + GNSS solutions. Finally, we checked the accumulated value of LoD. The lower the LoD drifts away, the more stable the solution. A positive impact of the addition of SLR observations to the GNSS data on the cumulative value of LoD was indicated by Bury et al. (2021). Let us now check if the change of the GNSS and SLR network constraining and the modification of the approach for the SLR RBs influence the cumulative value of LoD. Figure 13 depicts the accumulated values of the LoD drift for chosen solutions. In the case of the solution *C*1*G*, in which the RBs are dominated by the SLR observations, the drift is at a similar level of −4.7 ms/year as in the solution *M*1 (−4.9 ms/year). For the solution *C*1*L,* the SLR-to-LAGEOS observation applied for the RBs calculation slightly diminish the drift, yet the impact of the GNSS observations in the RBs makes the drift higher (−4.2 ms/year) than in the case of the other combined solutions with the basic approach to RBs for which the drift of the accumulated LoD does not exceed −4 ms/year. The network constraining seems to have a secondary impact on the stability of LoD determination. Even for the solution *G*1 with an unconstrained SLR network, the drift of LoD is at the level of −3.9 ms/year (same as for *C*3, *C*4, and *C*5, not shown here). The most stable are the solutions *C*1 and *C*2, for which the drift is at the level of −3.7 ms/year.

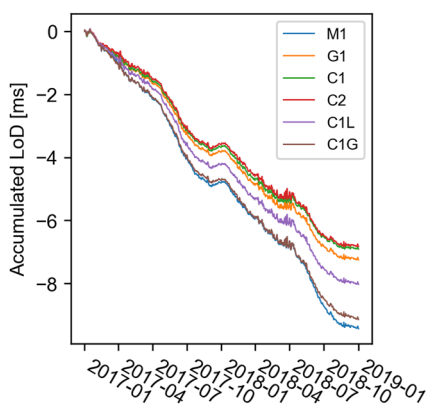

Figure 13. Accumulated LoD values with respect to the IERS C04 for all the test cases.

4. Conclusions

Laser retroreflectors mounted on the GNSS satellites enable us to conduct the co-location of two space techniques onboard navigation satellites, and therefore, the realization of TRF by a connection in space. In this study, we found the best strategy for TRF realization using combined GNSS and SLR station networks. We combined GNSS and SLR-to-GNSS observations to investigate the quality of the inter-technique linkage onboard the GNSS satellites and evaluate the impact of combined GNSS + SLR observations on the global geodetic parameters.

The best results in terms of TRF realization and, therefore for the estimation of the station position, formal errors, and coordinate repeatability are obtained when imposing the NNT and NNR constraints on the core stations of GNSS and SLR networks ($C1$). Other types of constraints imposed on either GNSS or SLR network ($C2$, $C3$, $C4$) also allow for estimating the station coordinates with relatively good quality. However, in terms of the GNSS network, one has to be aware that in the case of the solutions $C2$ and $C3$ when GCC are not estimated, the estimated GNSS station coordinates contain the geocenter motion signal and the limitation of the GNSS technique to sense the TRF origin and thus the quality of the determined positions is slightly worse than in the case of solutions $C1$, $C4$, and $G1$, in which the GCC is estimated.

In terms of the SLR network, when the rotation is not constrained, the orientation of the SLR network cannot reliably be transferred from the GNSS network. Therefore, besides solution $C1$, solution $C3$ without the GCC estimation can also be considered reliable. In terms of solution $G1$, the SLR network is unconstrained; hence it is calculated based on GNSS-microwave and SLR-to-GNSS observations. As a result in $G1$, we obtain a completely different result to the a priori realization of the SLR frame. This realization is not necessarily incorrect, as the quality of the determined SLR station coordinates is at a similar level as for the other combined solutions.

We calculated the linkage between co-located GNSS and SLR stations for those GNSS and SLR stations that tracked Galileo and GLONASS satellites based on the estimated station coordinates. Within the two years, the space ties were calculated in over 60% of 1-day solutions for the best-performing stations. The linkage in space between SLR and GNSS techniques can be determined with the accuracy of 34 mm (WTZZ-8834) and is independent of the ground measurements of local ties. As a result, the space ties might be used as an independent control for the *in situ* measurements or can serve as an additional observation with full variance-covariance information provided by the SLR-to-GNSS observation geometry for the realization of TRF.

The quality of the local ties was improved by the modification of handling of the SLR-to-GNSS RBs when considering SLR-to-LAGEOS and GNSS observations. The modified approach to SLR RBs applied in the solution $C1L$ has the greatest impact on the Up component of the space ties. The overall accuracy of the space ties was improved from 34 to 23 mm for pair WTZZ-8834. Moreover, the scale of the SLR network has changed w.r.t to the SLR network scale from solution $C1$. The effect of the scale change corresponds to 16 mm at the equator. Apart from the scale change, the modified SLR RBs introduce a translation of the SLR network between $C1L$ and $C1$. An additional effect is revealed in GCC. Although the network translation results and GCC seem to have a similar nature, the two effects neither can be summed up nor indicate which of the two solutions is better. However, solution $C1L$ indicates a better agreement with the *in situ* measurements in terms of the local ties, and the GCC from $C1L$ are closer to the zero value than those from solution $C1$ which indicates a larger offset and STD of GCC time series than $C1L$.

In terms of the global geodetic parameters, the addition of the SLR observations to GNSS satellites in the majority does not introduce major changes of the estimated GCC or ERPs compared to the GNSS-only solutions. In terms of GCC, the modeling of the GNSS orbits plays the central role, especially the direct solar radiation pressure. As for the ERPs, the time series is dominated by the GNSS, which is considered to be the most appropriate technique for the delivery of the ERPs. The only significant differences are recorded for the LoD parameter. First of all, the addition of the SLR-to-GNSS observations improves an offset and STD of the determined LoD. Moreover, the drift of the accumulated LoD, which can be an indicator of a stable solution, is lowest for the solution $C1$, that is, −3.7 mm/year as compared to the GNSS-only $M1$ solution for which the drift is at the level of −4.9 mm/year. Nevertheless, for the estimation of the global geodetic parameters, it is rather the satellite constellation that matters, not the type of space geodetic technique which provides the observations. Moreover, the good information is the fact that the co-location onboard

GNSS satellites using combined GNSS and SLR-to-GNSS observations does not harm the determined global geodetic parameters.

Despite the relatively small number of range measurements compared to the GNSS observations, the co-location onboard GNSS satellites is feasible; therefore, the TRF can be materialized, and the linkage between co-located stations can be successfully calculated. The strength of the connection onboard GNSS satellites in terms of STD is 40–50 mm in 1-day solutions for individual stations, whereas the mean values based on long time series agree to 3–4 millimeters with local tie measurements. The level of agreement is at a remarkable level when considering the relatively large size of the LRA mounted on GNSS satellites and the precision of the SLR measurements. The solution, which considers the modified SLR RBs (*C1L*) provides the most reliable results in terms of the realization of TRF providing independence from a priori local ties. The co-location onboard satellites might replace the TRF connection on the ground, yet the number of SLR observations and calculated data arc to GNSS satellites should be increased on an operational basis. It is planned that future Galileo satellites will broadcast the signal at VLBI frequencies, which will allow the co-location of three space geodetic techniques onboard one satellite constellation.

Data Availability Statement

The GNSS and SLR observations used for this study can be freely downloaded from the Crustal Dynamics Data Information System https://cddis.nasa.gov/Data_and_Derived_Products/CreateNetrcFile.html. The metadata for the Galileo satellites is provided by the GSA https://www.gsc-europa.eu/. Local ties values are provided by the ILRS site logs.

Acknowledgments
This work was funded by the National Science Centre (NCN), Poland. G. Bury, K. Sośnica, R. Zajdel, and D, Strugarek are supported by the grant UMO-2019/35/B/ST10/00515. We also thank the Wroclaw Center of Networking and Supercomputing computational grant using Matlab Software License No: 101979 (http://www.wcss.wroc.pl). The IGS MGEX is acknowledged for providing multi-GNSS data. We thank the ILRS for organizing GNSS tracking campaigns.

References

Abbondanza, C., Chin, T. M., Gross, R. S., Heflin, M. B., Parker, J. W., Soja, B. S., et al. (2017). JTRF2014, the JPL Kalman filter and smoother realization of the International Terrestrial Reference System: JTRF2014. *Journal of Geophysical Research: Solid Earth*, *122*(10), 8474–8510. https://doi.org/10.1002/2017JB014360

Altamimi, Z., Rebischung, P., Métivier, L., & Collilieux, X. (2016). ITRF2014: A new release of the International Terrestrial Reference Frame modeling nonlinear station motions: ITRF2014. *Journal of Geophysical Research: Solid Earth*, *121*(8), 6109–6131. https://doi.org/10.1002/2016JB013098

Anderson, J. M., Beyerle, G., Glaser, S., Liu, L., Männel, B., Nilsson, T., et al. (2018). Simulations of VLBI observations of a geodetic satellite providing co-location in space. *Journal of Geodesy*, *92*(9), 1023–1046. https://doi.org/10.1007/s00190-018-1115-5

Appleby, G., Rodríguez, J., & Altamimi, Z. (2016). Assessment of the accuracy of global geodetic satellite laser ranging observations and estimated impact on ITRF scale: Estimation of systematic errors in LAGEOS observations 1993–2014. *Journal of Geodesy*, *90*(12), 1371–1388. https://doi.org/10.1007/s00190-016-0929-2

Bizouard, C., Lambert, S., Gattano, C., Becker, O., & Richard, J.-Y. (2019). The IERS EOP 14C04 solution for Earth orientation parameters consistent with ITRF 2014. *Journal of Geodesy*, *93*(5), 621–633. https://doi.org/10.1007/s00190-018-1186-3

Boehm, J., Werl, B., & Schuh, H. (2006). Troposphere mapping functions for GPS and very long baseline interferometry from European Centre for Medium-Range Weather Forecasts operational analysis data: TROPOSPHERE MAPPING FUNCTIONS FROM ECMWF. *Journal of Geophysical Research*, *111*(B2). https://doi.org/10.1029/2005JB003629

Bruni, S., Rebischung, P., Zerbini, S., Altamimi, Z., Errico, M., & Santi, E. (2018). Assessment of the possible contribution of space ties onboard GNSS satellites to the terrestrial reference frame. *Journal of Geodesy*, *92*(4), 383–399. https://doi.org/10.1007/s00190-017-1069-z

Bury, G., Sośnica, K., & Zajdel, R. (2019). Multi-GNSS orbit determination using satellite laser ranging. *Journal of Geodesy*, *93*(12), 2447–2463. https://doi.org/10.1007/s00190-018-1143-1

Bury, G., Sośnica, K., Zajdel, R., & Strugarek, D. (2020). Toward the 1-cm Galileo orbits: Challenges in modeling of perturbing forces. *Journal of Geodesy*, *94*(2), 16. https://doi.org/10.1007/s00190-020-01342-2

Bury, G., Sośnica, K., Zajdel, R., Strugarek, D., & Hugentobler, U. (2021). Determination of precise Galileo orbits using combined GNSS and SLR observations. *GPS Solutions*, *25*(1), 11. https://doi.org/10.1007/s10291-020-01045-3

Dach, R., Lutz, S., Walser, P., & Fridez, P. (2015). *Bernese GNSS software version 5.2*. https://doi.org/10.7892/BORIS.72297

Desai, S. D. (2002). Observing the pole tide with satellite altimetry. *Journal of Geophysical Research*, *107*(C11), 3186. https://doi.org/10.1029/2001JC001224

Ferland, R., & Piraszewski, M. (2009). The IGS-combined station coordinates, earth rotation parameters and apparent geocenter. *Journal of Geodesy*, *83*(3–4), 385–392. https://doi.org/10.1007/s00190-008-0295-9

Glaser, S., Fritsche, M., Sośnica, K., Rodríguez-Solano, C. J., Wang, K., Dach, R., et al. (2015). Validation of components of local ties. In T. van Dam (Ed.), REFAG 2014 (Vol. 146, pp. 21–28). Springer International Publishing. https://doi.org/10.1007/1345_2015_190

Glaser, S., König, R., Neumayer, K. H., Nilsson, T., Heinkelmann, R., Flechtner, F., & Schuh, H. (2019). On the impact of local ties on the datum realization of global terrestrial reference frames. *Journal of Geodesy*, *93*(5), 655–667. https://doi.org/10.1007/s00190-018-1189-0

Glaser, S., Michalak, G., Männel, B., König, R., Neumayer, K. H., & Schuh, H. (2020). Reference system origin and scale realization within the future GNSS constellation "Kepler". *Journal of Geodesy*, *94*(12), 117. https://doi.org/10.1007/s00190-020-01441-0

Hadas, T., Krypiak-Gregorczyk, A., Hernández-Pajares, M., Kaplon, J., Paziewski, J., Wielgosz, P., et al. (2017). Impact and implementation of higher-order ionospheric effects on precise GNSS applications: Higher-order ionospheric effects in GNSS. *Journal of Geophysical Research: Solid Earth*, *122*(11), 9420–9436. https://doi.org/10.1002/2017JB014750

Johnston, G., Riddell, A., & Hausler, G. (2017). The International GNSS Service. In P. J. G. Teunissen, & O. Montenbruck (Eds.), *Springer handbook of global navigation satellite systems* (pp. 967–982). Springer International Publishing. https://doi.org/10.1007/978-3-319-42928-1_33

Klopotek, G., Hobiger, T., Haas, R., & Otsubo, T. (2020). Geodetic VLBI for precise orbit determination of Earth satellites: A simulation study. *Journal of Geodesy*, *94*(6), 56. https://doi.org/10.1007/s00190-020-01381-9

Kodet, J., Schreiber, K. U., Eckl, J., Plötz, C., Mähler, S., Schüler, T., et al. (2018). Co-location of space geodetic techniques carried out at the Geodetic Observatory Wettzell using a closure in time and a multi-technique reference target. *Journal of Geodesy*, *92*(9), 1097–1112. https://doi.org/10.1007/s00190-017-1105-z

Luceri, V., Pirri, M., Rodríguez, J., Appleby, G., Pavlis, E. C., & Müller, H. (2019). Systematic errors in SLR data and their impact on the ILRS products. *Journal of Geodesy*, *93*(11), 2357–2366. https://doi.org/10.1007/s00190-019-01319-w

Lyard, F., Lefevre, F., Letellier, T., & Francis, O. (2006). Modelling the global ocean tides: Modern insights from FES2004. *Ocean Dynamics*, *56*(5–6), 394–415. https://doi.org/10.1007/s10236-006-0086-x

Männel, B., & Rothacher, M. (2017). Geocenter variations derived from a combined processing of LEO- and ground-based GPS observations. *Journal of Geodesy*, *91*(8), 933–944. https://doi.org/10.1007/s00190-017-0997-y

Meindl, M., Beutler, G., Thaller, D., Dach, R., & Jäggi, A. (2013). Geocenter coordinates estimated from GNSS data as viewed by perturbation theory. *Advances in Space Research*, *51*(7), 1047–1064. https://doi.org/10.1016/j.asr.2012.10.026

Mendes, V. B., & Pavlis, E. C. (2004). High-accuracy zenith delay prediction at optical wavelengths. *Geophysical Research Letters*, *31*(14), L14602. https://doi.org/10.1029/2004GL020308

Otsubo, T., Appleby, G. M., & Gibbs, P. (2001). Glonass Laser Ranging Accuracy With Satellite Signature Effect. *Surveys in Geophysics*, *22*(5/6), 509–516. https://doi.org/10.1023/A:1015676419548

Pavlis, N. K., Holmes, S. A., Kenyon, S. C., & Factor, J. K. (2012). The development and evaluation of the Earth Gravitational Model 2008 (EGM2008): THE EGM2008 Earth gravitational model. *Journal of Geophysical Research*, *117*(B4). https://doi.org/10.1029/2011JB008916

Pearlman, M. R., Noll, C. E., Pavlis, E. C., Lemoine, F. G., Combrink, L., Degnan, J. J., et al. (2019). The ILRS: Approaching 20 years and planning for the future. *Journal of Geodesy*, *93*(11), 2161–2180. https://doi.org/10.1007/s00190-019-01241-1

Petit, G., & Luzum, B. (2010). *IERS conventions (technical note : 36)*. : Verlag des Bundesamts für Kartographie und Geodäsie.

Pinzón, I. H., & Rothacher, M. (2020). *Co-location of space geodetic techniques: Studies on intra-technique short baselines*. Springer Berlin Heidelberg. https://doi.org/10.1007/1345_2020_95

Prange, L., Villiger, A., Sidorov, D., Schaer, S., Beutler, G., Dach, R., & Jäggi, A. (2020). Overview of CODE's MGEX solution with the focus on Galileo. *Advances in Space Research*, *66*(12), 2786–2798. https://doi.org/10.1016/j.asr.2020.04.038

Ray, J., Rebischung, P., & Griffiths, J. (2017). IGS polar motion measurement accuracy. *Geodesy and Geodynamics*, *8*(6), 413–420. https://doi.org/10.1016/j.geog.2017.01.008

Rebischung, P., Altamimi, Z., Ray, J., & Garayt, B. (2016). The IGS contribution to ITRF2014. *Journal of Geodesy*, *90*(7), 611–630. https://doi.org/10.1007/s00190-016-0897-6

Sarti, P., Abbondanza, C., & Altamimi, Z. (2013). Local ties and co-location sites: Some considerations after the release of ITRF2008. In Z. Altamimi, & X. Collilieux (Eds.), Reference frames for applications in geosciences (Vol. 138, pp. 75–80). Springer Berlin Heidelberg. https://doi.org/10.1007/978-3-642-32998-2_13

Scherneck, H.-G. (1991). A parametrized solid earth tide model and ocean tide loading effects for global geodetic baseline measurements. *Geophysical Journal International*, *106*(3), 677–694. https://doi.org/10.1111/j.1365-246X.1991.tb06339.x

Sośnica, K., Bury, G., & Zajdel, R. (2018). Contribution of Multi-GNSS constellation to SLR-derived terrestrial reference frame. *Geophysical Research Letters*, *45*(5), 2339–2348. https://doi.org/10.1002/2017GL076850

Sośnica, K., Bury, G., Zajdel, R., Strugarek, D., Drożdżewski, M., & Kazmierski, K. (2019). Estimating global geodetic parameters using SLR observations to Galileo, GLONASS, BeiDou, GPS, and QZSS. *Earth, Planets and Space*, *71*(1), 20. https://doi.org/10.1186/s40623-019-1000-3

Sośnica, K., Zajdel, R., Bury, G., Bosy, J., Moore, M., & Masoumi, S. (2020). Quality assessment of experimental IGS multi-GNSS combined orbits. *GPS Solutions*, *24*(2), 54. https://doi.org/10.1007/s10291-020-0965-5

Steigenberger, P., Thoelert, S., & Montenbruck, O. (2018). GNSS satellite transmit power and its impact on orbit determination. *Journal of Geodesy*, *92*(6), 609–624. https://doi.org/10.1007/s00190-017-1082-2

Strugarek, D., Sośnica, K., Arnold, D., Jäggi, A., Zajdel, R., Bury, G., & Drożdżewski, M. (2019). Determination of global geodetic parameters using satellite laser ranging measurements to sentinel-3 satellites. *Remote Sensing*, *11*(19), 2282. https://doi.org/10.3390/rs11192282

Thaller, D., Dach, R., Seitz, M., Beutler, G., Mareyen, M., & Richter, B. (2011). Combination of GNSS and SLR observations using satellite co-locations. *Journal of Geodesy*, *85*(5), 257–272. https://doi.org/10.1007/s00190-010-0433-z

Thaller, D., Sośnica, K., Dach, R., Jäggi, A., Beutler, G., Mareyen, M., & Richter, B. (2014). Geocenter Coordinates from GNSS and Combined GNSS-SLR Solutions Using Satellite Co-locations. In C. Rizos, & P. Willis (Eds.), Earth on the edge: Science for a sustainable planet (Vol. 139, pp. 129–134). Springer Berlin Heidelberg. https://doi.org/10.1007/978-3-642-37222-3_16

Thaller, D., Sośnica, K., Steigenberger, P., Roggenbuck, O., & Dach, R. (2015). Pre-combined GNSS-SLR Solutions: What Could be the Benefit for the ITRF? In T. van Dam (Ed.), REFAG 2014 (Vol. 146, pp. 85–94). Springer International Publishing. https://doi.org/10.1007/1345_2015_215

Wielicki, B. A., Barkstrom, B. R., Harrison, E. F., Lee, R. B., Louis Smith, G., & Cooper, J. E. (1996). Clouds and the Earth's Radiant Energy System (CERES): An Earth observing system experiment. *Bulletin of the American Meteorological Society*, *77*(5), 853–868. https://doi.org/10.1175/1520-0477(1996)077<0853:CATERE>2.0.CO;2

Wilkinson, M., Schreiber, U., Procházka, I., Moore, C., Degnan, J., Kirchner, G., et al. (2019). The next generation of satellite laser ranging systems. *Journal of Geodesy*, *93*(11), 2227–2247. https://doi.org/10.1007/s00190-018-1196-1

Wu, X., Ray, J., & van Dam, T. (2012). Geocenter motion and its geodetic and geophysical implications. *Journal of Geodynamics*, *58*, 44–61. https://doi.org/10.1016/j.jog.2012.01.007

Zajdel, R., Sośnica, K., & Bury, G. (2017). A new online service for the validation of multi-GNSS orbits using SLR. *Remote Sensing*, *9*(10), 1049. https://doi.org/10.3390/rs9101049

Zajdel, R., Sośnica, K., & Bury, G. (2021). Geocenter coordinates derived from multi-GNSS: A look into the role of solar radiation pressure modeling. *GPS Solutions*, *25*(1), 1. https://doi.org/10.1007/s10291-020-01037-3

Zajdel, R., Sośnica, K., Dach, R., Bury, G., Prange, L., & Jäggi, A. (2019b). Network effects and handling of the geocenter motion in multi-GNSS processing. *Journal of Geophysical Research: Solid Earth*, *124*(6), 5970–5989. https://doi.org/10.1029/2019JB017443

Zajdel, R., Sośnica, K., Drożdżewski, M., Bury, G., & Strugarek, D. (2019a). Impact of network constraining on the terrestrial reference frame realization based on SLR observations to LAGEOS. *Journal of Geodesy*, *93*(11), 2293–2313. https://doi.org/10.1007/s00190-019-01307-0